Study of vector boson polarisation in the scattering of two W bosons with equal charge with the ATLAS detector at the LHC

Bachelor-Arbeit
zur Erlangung des Hochschulgrades
Bachelor of Science
im Bachelor-Studiengang Physik

vorgelegt von

Maren Bühring
geboren am 24.09.1998 in Hannover

Institut für Kern- und Teilchenphysik
Fakultät Physik
Bereich Mathematik und Naturwissenschaften
Technische Universität Dresden
2020

Eingereicht am 01. Dezember 2020

1. Gutachter: Prof. Dr. Michael Kobel
2. Gutachter: Dr. Frank Siegert

Abstract

English:
One of the core elements of the Standard Model (SM) is the mechanism of Electroweak Symmetry Breaking (EWSB), which is connected to the Higgs mechanism and the way in which particles gain mass. The study of Vector Boson Scattering (VBS) is is a way to explore this mechanism as the contributions of vertices including the Higgs boson avoid a violation of unitarity. The delicate cancellations required by the SM are more visible in the cross-section of scattering of longitudinally polarised vector bosons, which makes this channel also potentially sensitive to contributions of physics beyond the Standard Model. The model independent approach of Effective Field Theories aims to show the effect at low energies of unknown physics taking place at high energies by systematically extending to the Standard Model Lagrangian. This thesis discusses polarisation in the VBS of two positive W^+ bosons in the fully leptonic decay channel. To validate the simulation data used for the study, the differential cross section as a function of the boson decay angle θ^*_W is compared to the analytical function. A disagreement is observed and investigated further by considering the influence of different reference frames. The thesis also briefly discusses an EFT that adds one of three dimension eight operators to the Standard Model Lagrangian. It is shown that within the simulation of the model these only affect vertices with specific polarizations as expected.

Deutsch:
Eines der Kernelemente des Standard Modells (SM) ist der Mechanismus der elektroschwachen Symmetriebrechung (EWSB), der mit dem Higgs Mechanismus und dem Weg vebrunden ist, auf dem Teilchen Masse erlangen. Untersuchungen der Streuung von Vektor Bosonen (VBS) sind eine Möglichkeit mehr über den Mechanismus zu erfahren, da die Beiträge von Vertices mit Beteiligung des Higgs Bosons eine Verletzung der Unitarität verhindern. Das empfindliche Gleichgewicht das für das SM notwendig ist, ist im Wirkungsquerschnitt der VBS longitudinaler Bosonen besser zu erkenne, weshalb VBS auch potentiell sensitiv für Physik außerhalb des Standardmodells ist. Das Ziel einer modellunabhängigen Effektiven Feld Theorie ist es, die Effekte im niederenergetischen Bereich zu modellieren, die von neuer Physik bei sehr hohen Energien hervorgerufen werden. Dazu wird der Lagrange Operator des Standard Modells systematisch erweitert. In dieser Arbeit wird die Polarisation in VBS von zwei W^+ betrachtet, die vollständig leptonisch zerfallen. Um die Simulationsdaten zu validieren, die in dieser Studie verwendet werden, wird der differentielle Wirkungsquerschnitt in Abhängigkeit des Boson Zerfallswinkels θ^*_W mit der analytischen Erwartung verglichen und eine Differenz wird beobachtet. Diese wird weiter untersucht, indem der Einfluss unterschiedlicher Bezugssysteme in Betracht gezogen wird. Die Arbeit beschäftigt sich außerdem kurz mit einer möglichen EFT, die dem Lagrange Operator des Standardmodells einen von drei möglichen Operatoren der achten Dimension hinzufügt. Es wird gezeigt, dass innerhalb der verwendeten Simulationsdaten

wie erwartet die Operatoren nur Vertices mit bestimmten Polarisationen beeinflussen.

Inhaltsverzeichnis

1 Introduction

The Standard Model of particle physics is one of the most successful theories that are available to physicists today. It is able to make extensive and accurate predictions about three of the four fundamental forces, excluding gravity, which is described by the theory of general relativity. It is however, known to be imperfect. A unification of the Standard Model and the theory of general relativity to form a common description of all four interactions has not yet been achieved. There are also hypothesized phenomena like the existence of dark matter that are not yet explained by either theory.

One tool that has greatly impacted the development of theoretical and experimental particle physics since it was first turned on in 2008 is the Large Hadron Collider (LHC) [1]. It's four experiments ATLAS, CMS, ALICE and LHCb made experimental data accessible that enabled incredible progress in the understanding and validation of the Standard Model and the search for physics beyond it. One of the outstanding achievements of the LHC, as well as one of it's original goals, is the experimental discovery of a particle now strongly assumed to be the Higgs boson in 2012 [2].

One of the many processes that are used to further probe the accuracy, and possibly the limitations, of the Standard Model is the scattering of vector bosons. These processes are very closely linked to the exact mechanism of electroweak symmetry breaking and the Higgs mechanism, making them an access point to gather further information about these aspects of the Standard Model. Polarisation plays an important role in the studying of vector boson scattering, as a Standard Model without the Higgs boson would predict a violation of unitarity caused in the cross section of specifically the scattering of two longitudinally polarised bosons [3]. This study focuses on the polarisation aspect of the scattering process.

Vector boson scattering is not only a tool to better understand the Standard Model, it is also potentially sensitive to new physics beyond it. One of the ways to model this unknown physics is by using a bottom-up Effective Field Theory (EFT) approach. In this the Standard Model is assumed to be the low energy limit of a bigger theory that is then introduced by systematically adding higher order terms to the Lagrangian of the Standard Model to form an Effective Field Theory [4]. This thesis briefly considers three possible new operators and their relationship with the polarisation of the bosons involved. [5] As the polarisation of vector bosons is not a property that is easily accessible in experimental data, this thesis relies on simulation data produced by Monte Carlo generators. In these simulated events the properties of the decay products of the bosons are easily available, providing a way to visualize and understand the implications of the theory. This eventually aids in the development of experimental methods to make the key properties visible in real experimental data. Simulations can also be based on extensions of the Standard Model, like for example an EFT, making it possible to compare the expected results for both theories and therefore pointing in the direction of where to search for either the existence or the absence of evidence that the extended model does indeed accurately describe new physics.

1.1 The Standard Model of Particle Physics

The Standard Model of Particle Physics (Standard Model) describes three of the four fundamental interactions: the electromagnetic and the weak interaction, which can be combined into the electroweak interaction, and the strong interaction. The forces are expressions of fields that are governed by a local gauge symmetry, meaning that they remain invariant under a certain set of transformations. These symmetries can be written as

$$U(1)_Y \otimes SU(2)_L \otimes SU(3)_C \tag{1.1}$$

with the first two terms relating to the electroweak interaction and the last term referring to the strong interaction. All the fields have corresponding exchange particles called vector bosons. These include the photon for the electromagnetic, the gluon for the strong and the intermediate vector bosons $W^\pm$ and Z for the weak interaction. One thing all bosons have in common is an integer spin. This differentiates them from the other category of fundamental particles, the fermions. Electrons, muons, tauons, neutrinos and quarks are all fermions as they all have a half-integer spin.

Whether a particle participates in one of the three interactions is decided based on whether the particle possesses the necessary charge. For the electromagnetic interaction this refers to the electromagnetic charge, for the strong interaction to colour and for the weak interaction to the weak isospin. When combining the weak and the electromagnetic interactions, the electric charge and the weak isospin are combined into the weak hypercharge. Table 1.1 summarizes the fundamental particles and their charges. Photons can not interact with other photons through the electromagnetic interaction, as photons themselves do not carry electromagnetic charge. The intermediate vector bosons however do participate in the weak interaction, as they do carry the weak isospin. They can interact with each other both through triple and quartic vertices that include three and four vector bosons, respectively.

Whereas the photon does not have any mass, the $W^\pm$ and Z bosons do. They acquire their mass through a spontaneous breaking of the electroweak symmetry and the Brout–Englert–Higgs mechanism. This process requires the introduction of the Higgs field and it's corresponding boson, the Higgs boson. As the interactions between vector bosons are closely tied to electroweak symmetry breaking and the Higgs boson, the study of these processes offers insight into the details of the electroweak symmetry breaking. An introduction to the Standard Model and it's particles can be found in [6].

Table 1.1: Fundamental particles in the Standard Model and their charges. For fermions, the weak isospin depends on whether the particle is right- or left-handed.

Generation	Particle type	Particle	Electric charge Q	Color charge	Weak isospin I_3
i	Quark	u	2/3	Yes	LH: 1/2 RH: 0
	Quark	d	-1/3	Yes	LH: -1/2 RH: 0
	Lepton	e	-1	No	LH: -1/2 RH: 0
	Lepton	ν_e	0	No	LH: 1/2 RH: 0
ii	Quark	c	2/3	Yes	LH: 1/2 RH: 0
	Quark	s	-1/3	Yes	LH: -1/2 RH: 0
	Lepton	μ	-1	No	LH: -1/2 RH: 0
	Lepton	ν_μ	0	No	LH: 1/2 RH: 0
iii	Quark	t	2/3	Yes	LH: 1/2 RH: 0
	Quark	b	-1/3	Yes	LH: -1/2 RH: 0
	Lepton	μ	-1	No	LH: -1/2 RH: 0
	Lepton	ν_μ	0	No	LH: 1/2 RH: 0
Vector bosons	Boson	g	0	Yes	0
	Boson	γ	0	No	0
	Boson	Z	-1	No	0
	Boson	W	± 1	No	± 1
Scalar bosons	Boson	H	0	No	-1/2

1.2 Vector Boson scattering

There is no experiment available today that makes it possible to accelerate and collide vector bosons directly, so they need to be radiated off by other particles. In the LHC, the scattering is available indirectly through the $pp \to W^+W^+jj \to l^+l^+\nu\nu jj$ process: two quarks contained in the protons radiate off the vector bosons which then interact with each other, after which they decay into two lepton pairs each. With the two quarks propagating through to the final state, this means that the process is represented in the Feynman diagram 1.1. Different diagrams contribute to the actual interaction of the two vector bosons. The possible options depend on the charges of the vector bosons. To simplify this study, one configuration was chosen. As the fully leptonic channel of the scattering of two positive W bosons has been the first of these processes to be observed at the LHC [7], that process is discussed in this thesis. With two positive W bosons the possible diagrams that could fill the circle in figure 1.1 are shown in figure 1.2.

There is no s-channel vector boson or Higgs exchange contributions, as the necessary vertices do not follow the conservation of electromagnetic charge [8]. The positive charge also means

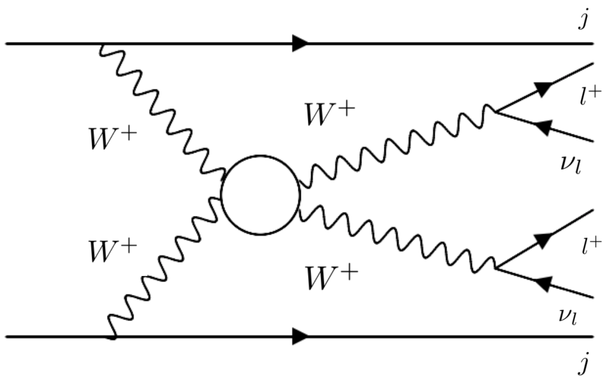

Figure 1.1: Feynman diagram of vector boson scattering for two W^+ bosons.

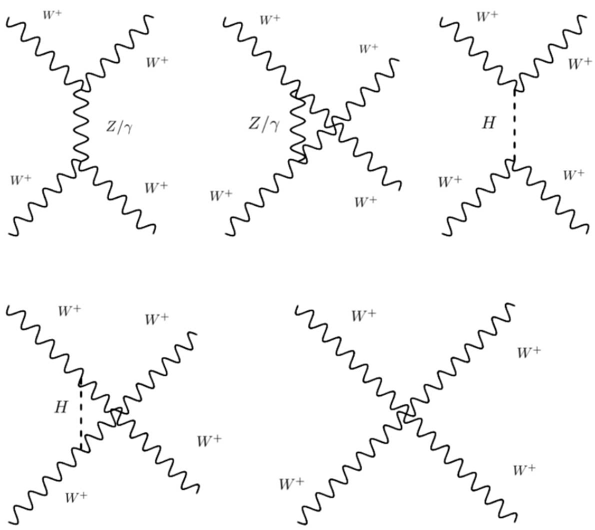

Figure 1.2: Possible vertices for $W^+W^+ \to W^+W^+$.

that after the VBS vertex the W^+ decay into either a e^+, μ^+ or τ^+ and the respective neutrino. In the case of one of the W^+ decaying into a tauon and a tauon neutrino, the tauon then decays further into a charged lepton and a neutrino, introducing even more neutrinos into the final state. This case also does not introduce any new details into the VBS aspect of the process. Of course the possibility of the W^+ decaying into a tauon would have to be considered in a study that involved experimental data, but as this thesis is based solely on simulation data, these cases will be excluded to simplify the analysis.

1.3 Polarization

1.3.1 Definition

A particle is referred to as polarized if it's spin has a preferred direction with respect to it's momentum. This is quantified using the helicity $h = \vec{S} \cdot \frac{\vec{p}}{|p|}$. For particles with a mass $m \neq 0$ like the vector bosons the helicity can take on one of three values: $h = \pm 1$, $h = 0$. Particles with a helicity of $h = 0$ are longitudinally polarized, in the other two cases the particle is transversally polarized. Among the two transversal polarizations $h = +1$ is referred to as right handed and $h = -1$ as left handed.
The definition of the helicity above includes the momentum vector $\vec{p}$, meaning that both the helicity and the polarization depend on the frame of reference.

1.3.2 Polarization in VBS

As stated in the introduction, polarization of vector bosons in VBS is interesting because electroweak symmetry breaking prevents a violation of unitarity in the scattering of longitudinally polarized vector bosons: The cross section of this process without the contribution of vertices including the Higgs boson increases with the center of mass energy until it violates the unitarity limit [9].
This implies that for the purpose of learning more about electroweak symmetry breaking the differentiation between longitudinal and transversal particles is more interesting than the one between right and left handed transversal particles. That is why in this thesis the notation of V_L for longitudinal particles and V_T for both right and left handed transversal particles will be used and the samples that are being considered include either longitudinal or transversal particles.
As the bosons quickly decay into stable particles, it is necessary to draw conclusions about the polarization of the original bosons from the properties of the final state particles.
To do this, the boson decay angle θ^*_W is introduced. It describes the angle between the charged lepton's momentum in the rest frame of the corresponding boson and the momentum of the boson boosted into a specific frame. This might be the rest frame of the two W^+ bosons, the Lab

frame or the Parton Parton rest frame, which is the rest frame of the initial state particles. The decay angle is connected to the polarisation of the W^+ boson due to conservation of angular momentum and the fact that the W^+ only couples to left-handed particles and right-handed antiparticles. While it is technically possible for the polarisations of the W^+ bosons to change during the scattering process, this effect is negligible in the scattering of two W^+ specifically [3].

If the frame that the boson's momentum is boosted into is identical to the frame that the helicity is defined in, the differential cross section of the polarisations is described by

$$\frac{1}{\sigma}\frac{d\sigma}{d\cos\theta_W^*} = f_{-1}\frac{3}{8}(1-\cos\theta_W^*)^2 + f_{+1}\frac{3}{8}(1+\cos\theta_W^*)^2 + f_0\frac{3}{4}sin^2\theta_W^* \qquad (1.2)$$

with the helicity fractions f_{+1}, f_{-1} and f_0 for right- and left-handed and longitudinal polarisations. This holds only as long as no lepton cuts are applied [10].

1.4 Effective Field Theories

The Standard Model has been very successful in predicting the experimental results produced by the LHC. It is however understood to have limitations, as there are effects that can not be explained by the Standard Model in it's current form. This includes issues like the potential existence of dark matter or the fact that there is currently no renormalizable quantum field theory of gravity [11]. The search for new physics continues using different approaches. One is to improve the accelerator and detector technology in hopes of reaching higher energies, luminosities and precision to directly search for new physics. Another approach is to do so indirectly. Effective Field Theories (EFT) are a way to search low energy areas that are accessible with experimental data for the effects of new physics that takes place at energies so high that they are currently out of reach experimentally [4].

The fundamental idea of an Effective Field Theory is to expand the Standard Model Lagrangian by adding terms that include operators of higher order. It therefore includes the Standard Model as a low energy limit [12]. The Standard Model Lagrangian includes operators up to the fourth dimension. There is different approaches to constructing the operators that will be added out of the Standard Model fields. One is to first develop a theory and then to work out the operators that reproduce the behaviour of the model. This top-down approach is difficult however, because it requires a fully formed theory and is specific to that particular model. Another possible approach to developing an EFT is the bottom-up approach. Here all operators that fit a minimum set of requirements are considered. This expansion aims to be model independent, which makes it very flexible [8].

Any Standard Model EFT Lagrangian can be written as [8]

$$\mathcal{L}_{\mathrm{EFT}} = \mathcal{L}_{\mathrm{SM}} + \frac{a_5}{\Lambda}\mathcal{O}^{(5)} + \sum_i \frac{a_i}{\Lambda^2}\mathcal{O}_i^{(6)} + \sum_j \frac{a_j}{\Lambda^4}\mathcal{O}_j^{(8)} + \dots \tag{1.3}$$

with the Standard Model Lagrangian $\mathcal{L}_{\mathrm{SM}}$. The operators $\mathcal{O}_j^{(n)}$ with $n > 4$ are constructed out of Standard Model Fields, are suppressed by the high energy mass scale Λ and have an unknown coupling a_j [12]. Bounds for these parameters can be found in detailed studies of both the theoretical predictions according to the EFT and the experimental data and it's current accuracy. The energy scale Λ plays the important role of marking the energy up to which direct searches are possible due to experimental access. As the Standard Model is assumed to be the low energy limit of the EFT, the new physics is certain to not take place at energies lower than Λ, as it would have already been seen in the experimental data.

In this thesis, three dimension eight operators are chosen and their individual influence on W^+ W^+ vector boson scattering is discussed. They were selected for two reasons: first, dimension eight operators are the lowest order to specifically impact four boson quartic vertices, and second they are expected to contribute to specific polarization modes. This thesis aims to validate this relation to polarization within the boundaries of this study.

It is important to mention that by only considering one dimension eight operator at a time, the couplings of all other EFT parameters are assumed to be zero, not only of operators with higher dimensions but also of all other dimension eight and dimension six and five operators. While the one possible dimension five operator does not have any impact on vector boson scattering at all, there are dimension six operators that do technically contribute to the process of vector boson scattering. Disregarding the contributions of these operators means to sacrifice the advantage of model independence, as that very specific selection of operators would correspond to an equally specific model. For this thesis, this is accepted for the sake of simplicity.

The chosen operators are

$$\mathcal{L}_{\mathrm{M},0} = -g^2 F_{\mathrm{M},0}\mathrm{tr}[(D_\mu H)^\dagger (D^\mu H)]\mathrm{tr}[W_{\nu\rho}W^{\nu\rho}] \tag{1.4}$$

$$\mathcal{L}_{\mathrm{S},1} = F_{\mathrm{S},1}\mathrm{tr}[(D_\mu H)^\dagger (D^\mu H)]\mathrm{tr}[(D_\nu H)^\dagger (D^\nu H)] \tag{1.5}$$

$$\mathcal{L}_{\mathrm{T},0} = g^4 F_{\mathrm{T},0}\mathrm{tr}[W_{\mu\nu}W^{\mu\nu}]\mathrm{tr}[W_{\alpha\beta}W^{\alpha\beta}] \tag{1.6}$$

and stem from the list in chapter 3.4 in [12]. The values of the coupling constants were chosen according to [13].

1.5 Experimental Setup: The ATLAS detector at the LHC

The polarisation of W bosons in VBS is not a property that is directly accessible through experiments right now. In order to learn about this and many other aspects of particle accelerator experiments it is necessary to rely on simulations instead of real experimental data. However, the Monte Carlo generators and other simulation methods are limited by our knowledge of the exact processes happening both during and after the collision and in the detectors. Ultimately the only way to test if a theory represents reality is to compare it's predictions to actual experimental data. That is why even when working only with simulated events it is important to know about the experimental setup and it's strengths and limits in order to not lose sight of the final goal of finding a way to test the theory using measurements.

The process of VBS is only one very small aspect of the research that is made possible through the Large Hadron Collider (LHC) and it's experiments, one of which is the ATLAS experiment.

The LHC is a high energy hadron collider built by the CERN organization in an international collaboration. It is located in a 26.7 kilometre long ring shaped tunnel that had originally been constructed for the LEP machine. It is connected to the CERN accelorator complex that acts as injector [1]. The goal of the following sections is to give an overview of the detector and it's components in order to give an impression of the experimental data it can provide. The information is closely based on [14], which gives a much more detailed description.

The ATLAS detector has a global coordinate system to describe directions and positions within it. The origin of the coordinate system is defined to be the collision point of the two beams. The z-axis points along the beam axis, with positive z values defined to be in the A-side and negative values in the C-side. The x-y-plane is perpendicular to the beam axis with the positive side of the x-axis pointing upwards and the positive values of the y-axis pointing towards the center of the ring. Quantities like the transversal momentum p_t or the transversal energy E_t consist of the x and y components of the quantity. The angle around the beam axis (in the x-y-plane) is called ϕ and the angle in the z-x-plane is referred to as θ. The latter is also used to define the pseudo-rapidity $\eta = -\ln\tan(\theta/2)$. The rapidity $y = l\ln[(E + p_z)/(E - p_z)]$ is used mainly for objects with high masses like jets.

The detector is constructed concentrically around the beam axis with the inner detector wrapping around the collision area and the calorimeter system wrapped around the inner detector. Figure 1.3 shows an overview of the entire detector. One of the challenges in recording the data collected in the collisions is it's incredible amount. To avoid this issue, the detector is equipped with Trigger and Data Acquisition systems (collectively referred to as TDAQ), that process the data in several levels, to decide which events are definitely not relevant and which ones need to be recorded.

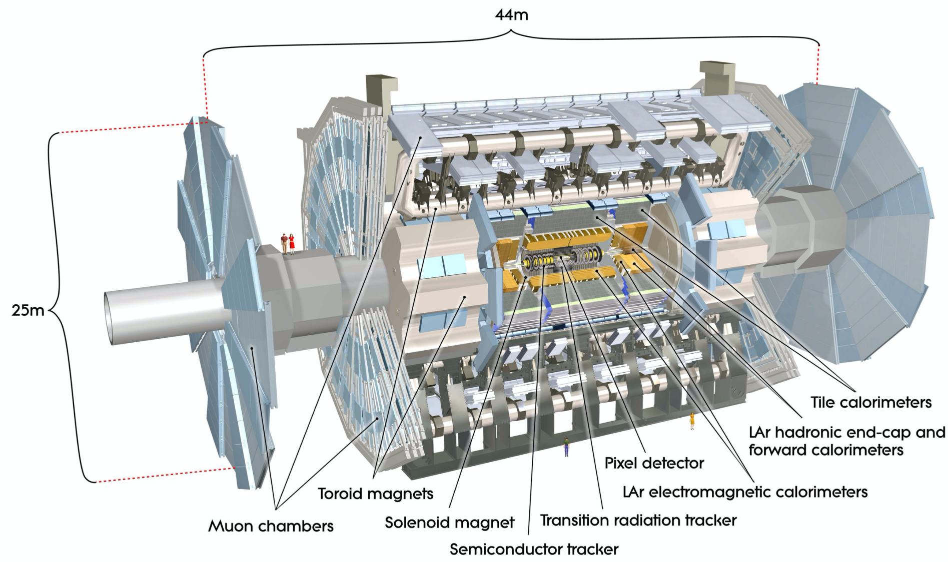

Figure 1.3: Cut-open view of the ATLAS detector from [14].

1.5.1 The inner detector

Figure 1.4 shows the components of the inner detector. It focuses on reconstructing vertices and particle tracks. It is immersed in a 2 T magnetic field and contained in a cylindrical envelope of 1150 mm radius.

The components closest to the beam are silicon pixel detectors. They have the highest granularity of all detectors and are accessible through approximately 80.4 million readout channels. A track typically crosses three pixel layers.

Outside of the pixel detectors the particle hits the SCT (Semi Conductor Tracker). It consists of strips of sensors that are arranged parallel to the beam direction and has approximately 6.3 million readout channels. A particle crossing the SCT hits eight layers of strips. Both the pixel detectors and the SCT cover a region with $|\eta| < 2.5$

The outer layer of the inner detector consists of 4 mm straw tubes that form the TRT (Transistion Radiation Tracker). In the barrel area they are arranged parallel to the beam and in the end-cap region they form wheels. The TRT enables track following up to $|\eta| = 2.0$ and has about 351,000 readout channels. A particle track typically triggers as many as 36 hits within the TRT.

1.5.2 The calorimeter system

Figure 1.5 shows the calorimeter system of the ATLAS detector. It consists of an electromagnetic calorimeter that aims to provide precision measurements of electrons and photons followed by several hadronic calorimeters with a coarser granularity that are used for jet reconstruction and E_t^{miss} measurements. For this purpose among other things it is important for

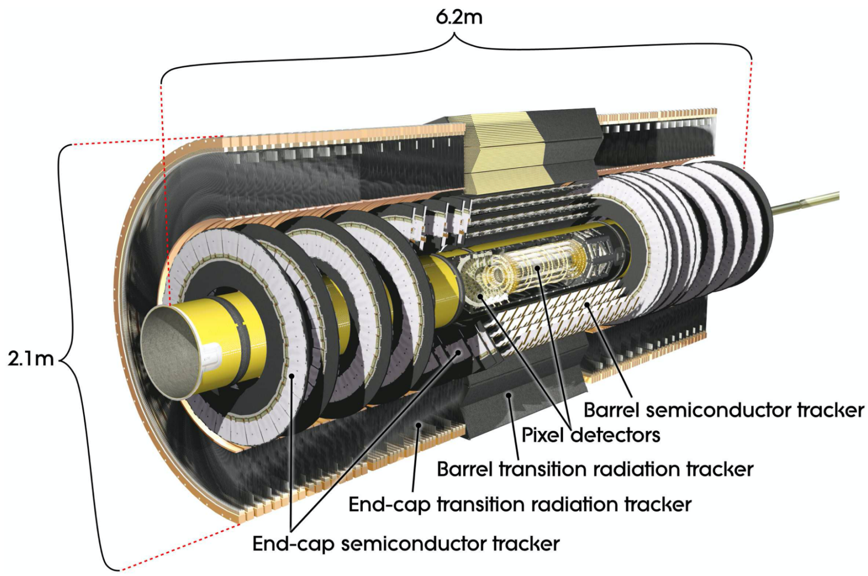

Figure 1.4: Cut-open view of the inner section of the ATLAS detector from [14].

the calorimeters to contain the electromagnetic and hadronic showers and limit punch-trough to the muon-system. To achieve this, the depth of the calorimeters is adjusted.

The layer closest to the inner detector is the electromagnetic calorimeter. It is a lead-LAr detector and has accordion-shaped kapton electrodes, which help to avoid azimuthal cracks, and lead absorber plates. In the eta region $|\eta| < 2.5$ that aims to provide high precision physics, the electromagnetic calorimeter is subdivided into three layers, whereas for the end-cap there is only two segments in depth and a coarser granularity.

In addition to the electromagnetic calorimeter there is also three hadronic calorimeters. The tile calorimeter wraps around the electromagnetic barrel and extends to also cover the LAr forward calorimeter and the hadronic and electromagnetic end-caps. that covers a region of $|\eta| < 1.7$. It uses steel as an absorber and scintillating tiles as the active material. It covers the radii between 2.28 m and 4.25 m. It is divided into 64 modules azimuthally and three layers in depth.

The second is the LAr hadronic end-cap calorimeter that sits right behind the the end-cap parts of the electromagnetic calorimeter. It consists of two independent wheels per side that are built from 32 identical wedge-shaped modules. It has an η range of $|\eta| < 3.2$ and deliberately overlaps with both the forward and the tile calorimeter. The wheels are made of copper of increasing thickness that is interleaved with gaps filled with LAr that acts as the active material.

Lastly there is the Forward calorimeter, which is included in the end-cap cryostats. It's front face is set back about 1.2 m to reduce neutron albedo in the inner detector cavity, which limits the possible detector depth and makes a high density design necessary. The Forward calorimeter is made up of three modules: a copper one designed predominantly for electromagnetic measurements and two tungsten elements for measuring hadronic showers.

1.5.3 The muon system

Because of the high mass of muons they travel through the calorimeter system without being slowed down to a stop in the process. This makes a seperate muon spectrometer necessary that wraps around the calorimeter system described above. It uses the deflection of muons in magnetic fields and is equipped with separate trigger system and tracking chambers. The magnetic field is supplied by both a large barrel toroid and two end-cap magnets, which together cover the region with $|\eta| < 2.7$. The resulting field is mostly orthogonal to the direction of the muon tracks.

One of the challenges in the design of the muon spectrometer is the high expected particle flux, which influence the performance parameters. The chambers of the spectrometer form three cylindrical layers around the beam axis in the barrel region, while being perpendicular to the beam axis in the end-cap regions.

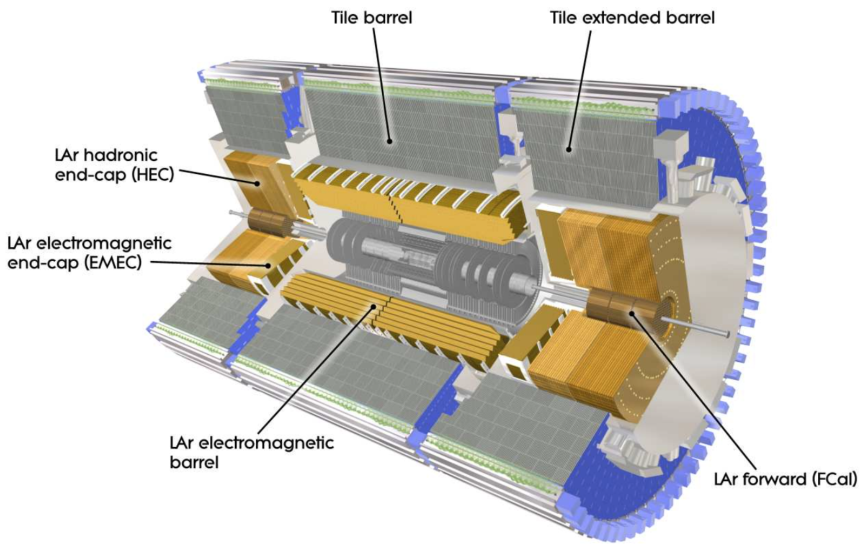

Figure 1.5: Cut-open view of the calorimeter system of the ATLAS detector from [14].

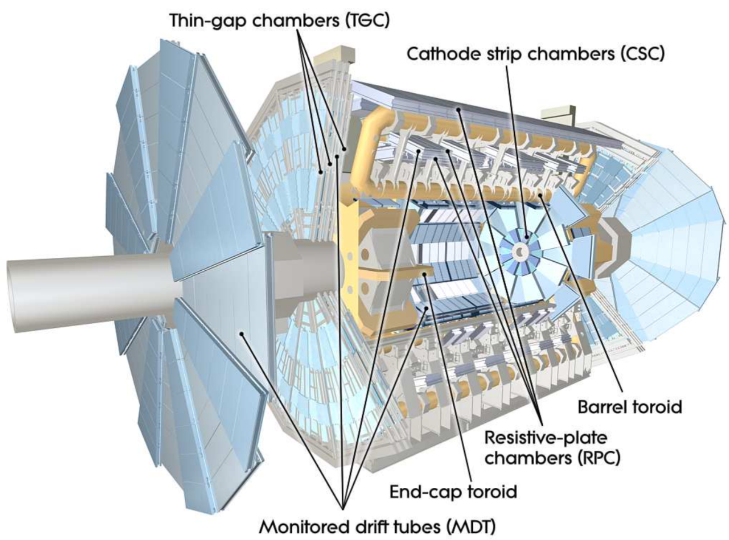

Figure 1.6: Cut-open view of the muon system of the ATLAS detector from [14].

2 Analysis and Results

2.1 Event Generation

The simulated events discussed in this thesis were generated using version 2.7.3 of the Monte Carlo generator MadGraph5_aMC@NLO (21.06.2020) [15]. The information needed to specify the details of the generation process is collected in the process card, the run card and the parameter card. The first one includes the process definition, which for the samples generated for this thesis are summarized in table 2.1. The run card includes the software parameters like the reference frame in which the matrix element for the polarizations is evaluated. This thesis refers to this reference frame as the one the samples were generated in. The run card also includes the generation cuts. For this study these are limited to the Cuts detailed in 2.2. The lepton cuts are set to not be applied to leptons that are decay products by choosing False = cut_decays in order to produce the total phase space without lepton cuts needed for this study. The parameter card defines important model parameters like particle masses shown in 2.3 and, in this case, EFT parameters. To enable the software to handle the inclusion of these EFT parameters, a model named SM_LS012_LM017_LT012_Ind5_UFO_June19.tar.gz [16], which is based on the paper [17], was used. For the samples labelled EFT one of the three operators listed in 1.4 was added by setting the corresponding parameter to the current upper limit for that parameter in the context of the same sign WW final state, with this analysis framework and at ATLAS [13]. The values are FT0 = 1.278, FM0 = 12.134 and FS1 = 56.476. The software is able to produce samples that represent the full $pp \rightarrow W^+W^+jj \rightarrow ll\nu\nu jj$ process, which are referred to as full in the following section, and samples that include two longitudinal, two transversal or exactly one longitudinal and one transversal W^+ boson, referred to as TT, LL and TL .Unfortunately, the production of LL and TL samples posed some technical difficulties. Ultimately a work-around could be found, but even with this solution the TT and TL samples generated in the WW rest frame did not appear to be trustworthy enough, which is why this thesis only includes TT samples generated in the WW rest frame. Another problem occured when trying to generate a mixed vertex sample (TL) including the EFT parameter FM0. The event generation had to be simplified to only include events with two opposite flavour leptons. In order to maintain as much comparability as possible the other M0 samples TT and LL were also limited to this easier process definition. The difference is detailed in 2.1. All samples include 100,000 events.

Table 2.1: Overview of the samples used in this thesis and their process definitions. The EFT column shows for which EFT parameters the sample was generated (SM meaning all EFT parameters set to zero). [Param] in the title of the sample is replaced with either SM, T0, or S1 and [*] is replaced by T0=1 or S1=1 depending on the parameters used.

Sample	Rest frame	Pol.	Process definition	EFT
[Param]_full	Does not apply	Mixed	generate p p > w+ w+ j j QCD=0 [*], w+ > e+ ve, w+ > mu+ vm @0 add process p p > w+ w+ j j QCD=0 [*], w+ > e+ ve @1 add process p p > w+ w+ j j QCD=0 [*], w+ > mu+ vm @1	SM, T0, S1
[Param]_wwrfr_TT	me_frame = 3, 4, 5, 6	TT	generate p p > w+T w+T j j QCD=0 [*], w+ > e+ ve, w+ > mu+ vm @0 add process p p > w+T w+T j j QCD=0 [*], w+ > e+ ve @1 add process p p > w+T w+T j j QCD=0 [*], w+ > mu+ vm @1	SM, T0, S1
[Param]_wwrfr_LL	me_frame = 3, 4, 5, 6	LL	generate p p > w+0 w+0 j j QCD=0 [*], w+ > e+ ve, w+ > mu+ vm @0 add process p p > w+0 w+0 j j QCD=0 [*], w+ > e+ ve @1 add process p p > w+0 w+0 j j QCD=0 [*], w+ > mu+ vm @1	SM, T0, S1
[Param]_wwrfr_TL	me_frame = 1, 2	TL	generate p p > w+T w+0 j j QCD=0, w+ > e+ ve, w+ > mu+ vm @0 add process p p > w+T w+0 j j QCD=0 [*], w+ > e+ ve @1 add process p p > w+T w+0 j j QCD=0 [*], w+ > mu+ vm @1	SM, T0, S1
M0_wwrfr_TT_of	me_frame = 1, 2	TT	generate p p > w+ w+ j j QCD=0 M0=1, w+ > e+ ve, w+ > mu+ vm @0	M0
M0_wwrfr_TT_of	me_frame = 1, 2	TT	generate p p > w+T w+T j j QCD=0 M0=1, w+ > e+ ve, w+ > mu+ vm @0	M0
M0_wwrfr_LL_of	me_frame = 1, 2	LL	generate p p > w+0 w+0 j j QCD=0 M0=1, w+ > e+ ve, w+ > mu+ vm @0	M0
M0_wwrfr_TL_of	me_frame = 1, 2	TL	generate p p > w+T w+0 j j QCD=0 M0=1, w+ > e+ ve, w+ > mu+ vm @0	M0

Table 2.2: Generation cuts included in the run card. For all minimal parameters not mentioned here the value is zero, for all maximum parameters not mentioned there is no cut (-1 in the MadGraph syntax).

Parameter	Value	Explanation
ptj	20.0	Minimum p_t for jets
ptl	10.0	Minimum p_t for charged leptons
etaj	5.0	Maximum jet rapidity
etal	2.5	Maximum lepton rapidity
drjj	0.4	Minimum distance between jets
drll	0.4	Minimum distance between leptons
drjj	0.4	Minimum distance between jets and leptons

Table 2.3: Particle masses in the parameter card used for the generation of events.

Particle	Mass in GeV/c^2
c, b, u, d, s, e^-, μ^-, γ, g, ν_e, ν_μ, ν_τ	0
τ^-	1.777
Z	91.188
W^+	80.419
H	125
t	172

2.2 Event Analysis

The analysis performed for this thesis is based on the Rivet framework. It was constructed on the basis of an already existing VBSCost analysis by the VBSCan COST Action [18] that also aimed to study VBS processes with two W bosons. It already included many of the basic event properties like the lepton and jet p_t and many others. Two different phase spaces were introduced to enable switching between the cuts included in the original analysis and the total phase space without any analysis cuts that is necessary for this study.

The most important parts that were added are aimed at the study of polarization in VBS specifically. Most of these additions relied on a different analysis by Carsten Bittrich that focuses on VBS of a W and a Z boson [3]. Elements like the calculation of the decay angles were adapted from this analysis to fit the existing VBSCost analysis and the situation with two W^+ bosons. The most important parts of the analysis are described in the following sections. The analysis operates on truth level only. All the particles included in the final state (two charged leptons, two neutrinos, two jets that are even accessible as quarks) and their properties are fully available. That is not the case for experimental data, where among other difficulties like misidentification and measurement uncertainties the neutrinos are only accessible through the missing transverse energy, which makes the reconstruction of the W^+ bosons from the final state particles much more difficult.

2.2.1 Matching of charged leptons and neutrinos

In order to reconstruct properties of the W^+ and quantities related to it like the decay angle it is necessary to choose one charged lepton and one neutrino from the list of final state particles that are presumed to be the decay product of a common W^+. This is achieved by first entering all final state particles that are either electrons or muons into a list ordered by descending transversal momentum p_t. The one with the highest p_t is then considered to be one of the decay products of the W boson W_1. To find the matching neutrino, these are also entered into a list. From this list of neutrinos the one is chosen that fits the flavor of the charged lepton and for which the resulting invariant mass of the charged lepton and the neutrino is closest to the W mass. The chosen neutrino is then removed from the list and the process is repeated for the charged lepton with the second highest p_t to form W_2.

The result is two particle couples that in the following analysis are assumed to be the decay particles of W_1 and W_2, respectively. The particle couples are referred to as W candidates for simplicity reasons in the following sections. Figure 2.1 shows the invariant masses of the W candidates for a sample of the full process generated in the WW rest frame. A clear peak at the mass of the W $m_W = 80.419 GeV/c^2$ is visible, indicating that the matching process was successful.

To assess the results of the analysis and to compare them with the analytical expectations

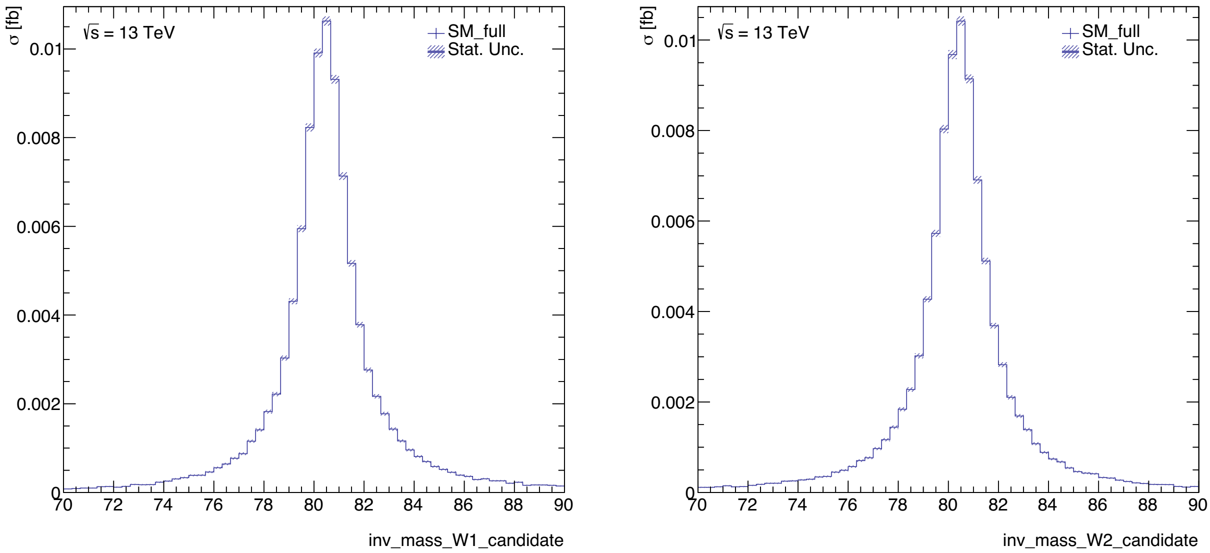

(a) **(b)**

Figure 2.1: Invariant mass in GeV of the reconstructed W^+ boson in W^+W^+ vector boson scattering. W1 is the reconstructed boson that decayed into the charged lepton with higher p_t (leading lepton) (a) and W2 the one that decays into the lower p_t lepton (subleading lepton) (b).

they are plotted in histograms. Plotting the results for the W_1 candidate in one histogram and those for the W_2 candidate in another introduces a bias: W_1 is always the candidate with the charged lepton with higher p_t between the two. That means that the distribution of lepton p_t for W_1 is not representative of the distribution for all leptons. To avoid this bias, the lepton candidates W_{closer} and $W_{further}$ are introduced. W_{closer} is the candidate closer to the W mass and $W_{further}$ the one further away from it.

2.2.2 Calculation of decay angles

The decay angle as introduced in section 2.2.1 is calculated in two different reference frames: the WW rest frame, and the Parton Parton rest frame. As described above, the decay angle is the angle between the charged lepton's momentum in the rest frame of the W boson and the momentum of the boson in the respective specific frame from the list above. On a practical level this is achieved by first boosting the lepton's momentum into the boson's rest frame. Then the z-axis of this frame is rotated to point in the direction of the boson's momentum boosted into the desired frame. To compare the results to the analytical function the cosine of the angle is calculated and plotted. Unfortunately the decay angle in the Parton Parton rest frame is not as easily accessible, as the initial state particles are not directly available to the analysis. Instead, the Parton Parton rest frame is reconstructed by adding up the four momenta of all the final state particles. The boson decay angle θ^*_W is referred to as ThetaCloser/FurtherNeutrino_WWRFr/PPRFr in the plots, indicating the boson, the reference frame that the angle is based on and the fact that it was calculated using the neutrino.

2.3 Results with SM samples

This section discusses the results for samples that were generated according to the Standard Model, so with all EFT parameters set to zero.

2.3.1 Comparing stacked polarizations to the full process

The generated event samples are divided into the polarizations. When adding up the cross sections of all the polarizations, they can be compared to the cross section of the full process. Figure 2.2 shows the stacked up polarizations in comparison to the full process for samples generated in the WW rest frame. It illustrates that while the stacked processes almost reach the cross section of the full process, there seems to be some missing contributions. This is probably because the process of generating samples that differentiate between the polarizations ignores the contributions of interferences between those processes, while those are included in the full process.

2.3.2 Decay angle plots

The polarization of the W bosons involved in a VBS process influences some properties of the decay products. Two of the most apparent examples are shown in figure 2.3. Both show a comparison between three samples generated in the WW rest frame, one with TT, one with LL and one with TL polarizations. The left plot shows the cosine of the decay angle discussed in 1.3.2. The three polarizations are very easily distinguishable. Another variable that allows for the polarizations to be distinguished from one another is the jet p_t as shown in the right plot for the jet with higher p_t j1. Specifically this variable allows a differentiation between the LL sample and the other two. Unfortunately both of these variables are not easily accessible through experimental data. The decay angle requires the reconstruction of the neutrino and the low jet p_t is often not available at detector level due to necessary cuts.
To verify whether the decay angle plots have the expected shape predicted by 1.2 the plots are compared to this analytical function. As the histograms shown here plot $\cos\theta^*$ on the x-axis, the fitting function can be expressed as

$$\frac{1}{\sigma}\frac{d\sigma}{dx} = f_{-1}\frac{3}{8}(1-x)^2 + f_{+1}\frac{3}{8}(1+x)^2 + f_0\frac{3}{4}(1-x^2) \qquad (2.1)$$

As mentioned before, the samples group together the events with left-handed and right-handed bosons in the TT samples, whereas the LL sample contains only events with two longitudinally polarized W bosons. That means that in the histogram for the TT sample a fit is necessary

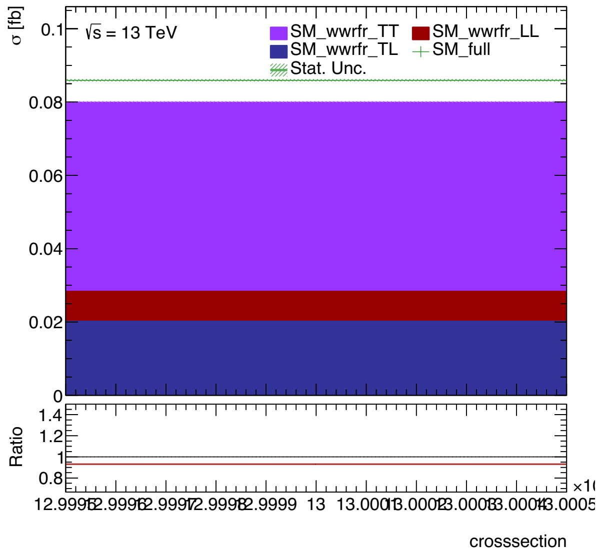

Figure 2.2: Stacked total cross sections of individual polarizations samples compared to the cross section of the full process. The polarization samples include vertices with either two longitudinal (LL), two transversal (TT) and mixed vertices (TL), whereas in the full sample the polarizations are not separated in the generation process.

to determine the share of events with right- and left handed bosons. This leads to the fitting function

$$\frac{1}{\sigma}\frac{d\sigma}{dx} = a * \frac{3}{8}(1-x)^2 + (1-a)\frac{3}{8}(1+x)^2 \tag{2.2}$$

with the fitting parameter a. The histograms for the decay angle in the WW rest frame for the TT sample generated in the WW rest frame is shown in figure 2.4. The figure includes plots for both W_{closer} and W_{further}. As mentioned in 2.2.1 this particular plotting method helps to avoid a bias in the lepton p_t. Comparing the two plots shows that there is no significant difference between the them. In the following sections only W_{closer} will be discussed, but it is always implied that W_{further} behaves in the same way. The result of the fit for W_{closer} is the fitting parameter $a = 0.3962 \pm 0.0019$, which implies that there are more events with right-handed than those with left-handed W bosons. The quality of the fit can be described using the reduced χ^2_{red} value. It is defined as the χ^2 divided by the number of degrees of freedom $\chi^2_{red} = \frac{\chi^2}{ndof}$. A value near 1 would indicate a good fit. For the fit performed here, the value is $\chi^2_{red} = 10.034$ meaning that there is a significant shape difference between the histogram and the fitting function. This difference in shape is more visible in the left plot of figure 2.5, which shows the same histogram and fit as the left plot of figure 2.4 but with a logarithmic y-axis. This emphasizes the shape difference and shows that towards $\cos(\theta^*) = -1$ and $\cos(\theta^*) = 1$ the fit is higher than the simulation data and around $\cos(\theta^*) = 0.2$ the fit is under the simulation data.

The right plot in figure 2.5 shows that a similar problem exists with the histogram that includes only events with two longitudinally polarized W bosons. As the LL sample only includes that one type of event, no fitting parameter is necessary for the analytical function: If the decay angle is calculated in the rest frame that the sample was generated in and no lepton cuts are applied, the distribution is expected to fit the analytical function

$$\frac{1}{\sigma}\frac{d\sigma}{dx} = \frac{3}{4}(1 - x^2) \tag{2.3}$$

As the figure shows, this is approximately the case, but there is a visible difference in shape. Towards $\cos(\theta^*) = 1$ and $\cos(\theta^*) = -1$ the analytical function is under the simulation data and around $\cos(\theta^*) = -0$ it is higher than the histogram. These shape differences in both the TT and the LL plots are discussed further in section 2.3.3.

Figure 2.6 shows histograms of both the sample with one transversal and one longitudinal W bosons and the full process. Events in both of these samples include W bosons of all polarizations, meaning that the full fitting function with two fitting parameters needs to be used.

$$\frac{1}{\sigma}\frac{d\sigma}{dx} = a * \frac{3}{8}(1 - x)^2 + b * \frac{3}{8}(1 + x)^2 + (1 - a - b) * \frac{3}{4}(1 - x^2) \tag{2.4}$$

For the left plot of figure 2.6 this results in the fitting parameters $a_{TL} = 0.2040 \pm 0.0027$ and $b_{TL} = 0.319 \pm 0.003$ with $\chi^2_{red} = 0.879$. The events in the TL sample are konwn to include exactly one longitudinal and one transversal boson. As the parameters represent the fraction of bosons with that particular polarization, the two parameters are expected to add up to 0.5, leaving the other half to be occupied by longitudinally polarized bosons. This is approximately the case, which together with the value for χ^2_{red} suggests that this is fit of much better quality than the ones for the LL and TL samples.

The same goes for the fit of the full process. Here, there is no previous knowledge of the fractions of different polarization except for the fact that they need to add up to one. The fit results in the parameters $a_{fulll} = 0.2757 \pm 0.0028$ and $b_{full} = 0.401 \pm 0.003$ with $\chi^2_{red} = 1.446$, which is also a better fit than the TT and LL ones. The parameters suggest that there is more transversal than longitudinal W bosons. This is supported by figure 2.2, in which it is visible that compared to the TL and LL sample, the TT sample has a higher cross section.

These more accurate fits for the TL and the full sample may be the result of the fact that the inaccuracies in the longitudinal and transversal parts of the samples cancel each other out: The TT sample is too low around $\cos(\theta^*) = \pm 1$ and too high for $\cos(\theta^*) = 0$, but the exact opposite is true for the LL sample. The issue of the bad fit agreement is investigated further in the next section.

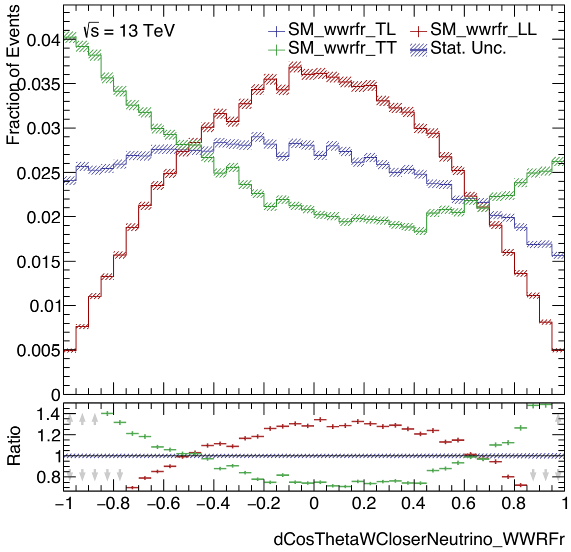

(a) Differential cross section as a function of the cos of the decay angle θ^*_W.

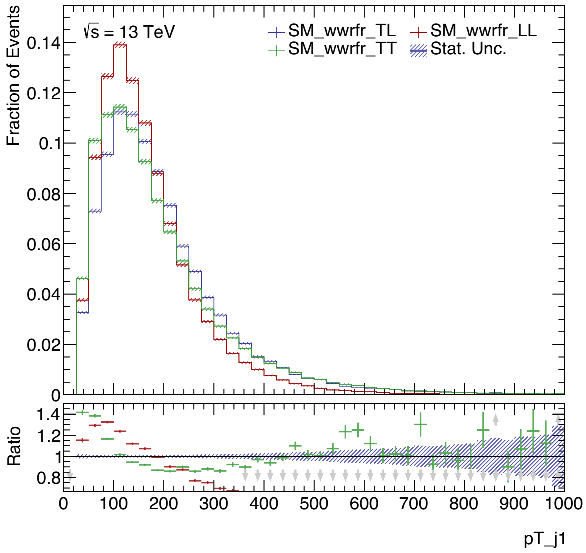

(b) Differential cross section as a function of the p_t in GeV of the jet with the highest p_t.

Figure 2.3: Comparison of samples containing longitudinal (LL), transversal (TT) and mixed (TL) polarization vertices of W^+W^+ vector boson scattering for different variables.

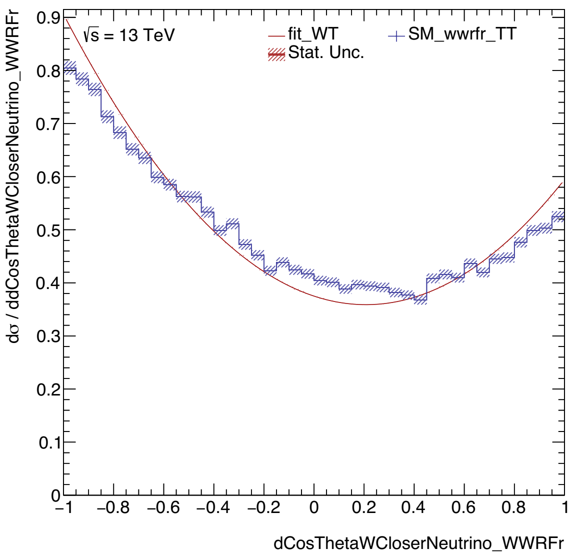

(a) Fit for W_{Closer}.

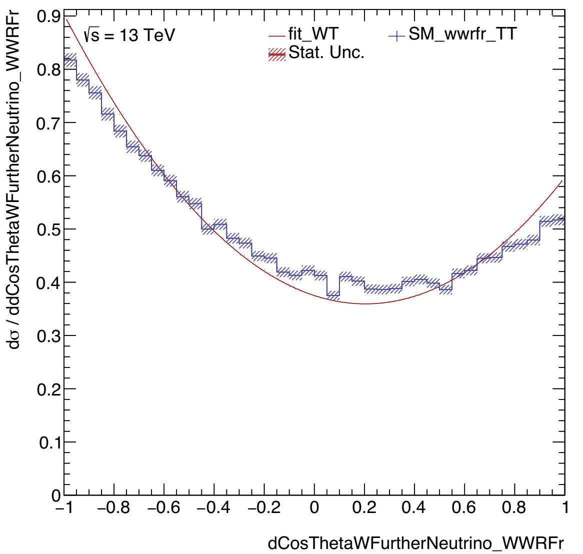

(b) Fit for W_{Further}.

Figure 2.4: Fitted differential cross section as a function of the cos of the decay angle θ^*_W for transversal W^+ bosons in W^+W^+ vector boson scattering. W_{Closer} is the reconstructed W^+ boson with whose invariant mass that is closer to the actual boson mass, and W_{Further} the one further away from it.

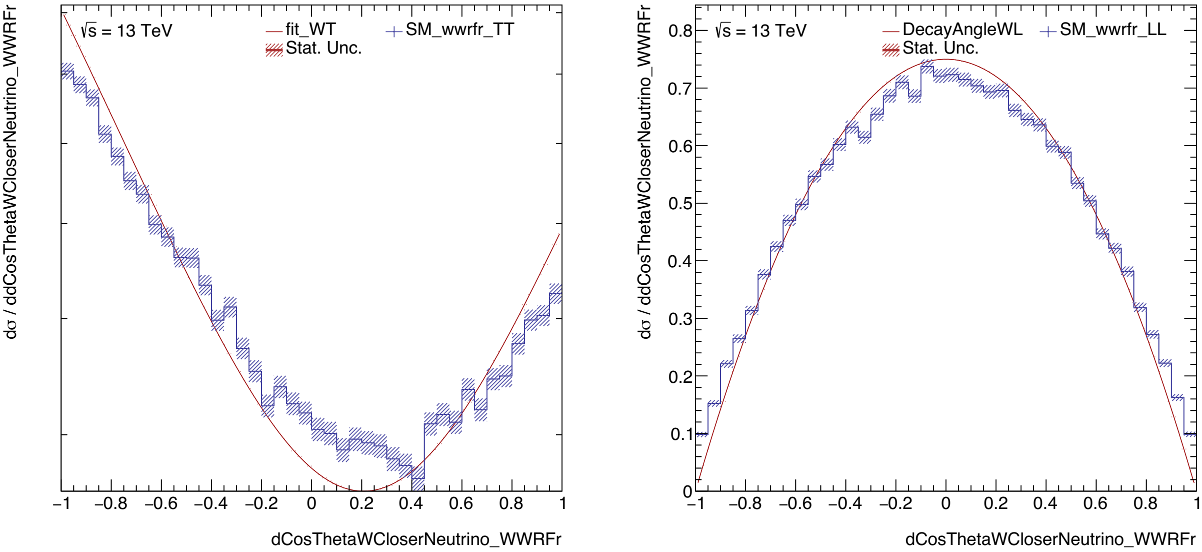

(a) Histogram and fit for sample with transversal vertices.

(b) Histogram and analytical function for sample with longitudinal vertices.

Figure 2.5: Differential cross section as a function of the cos of the decay angle θ^*_W for W^+ bosons in W^+W^+ vector boson scattering. The TT sample includes transversal vertices and the LL sample longitudinal ones. Also includes the analytical functions.

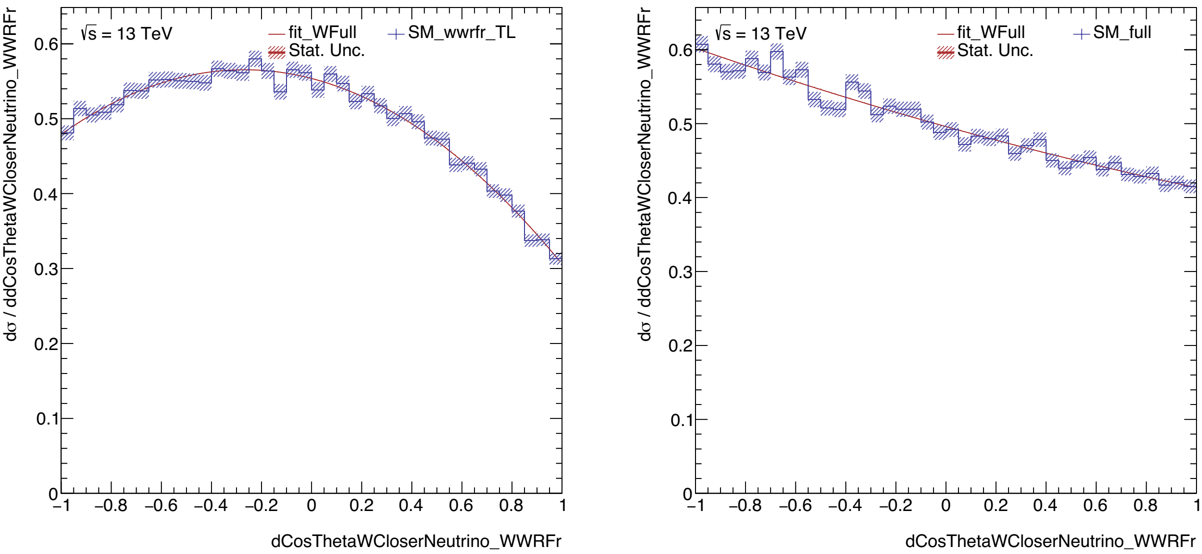

(a) Histogram and fit for mixed sample.

(b) Histogram and fit for the full process.

Figure 2.6: Differential cross section as a function of the cos of the decay angle θ^*_W for W^+ bosons in W^+W^+ vector boson scattering, including fitting functions. The TL sample includes vertices with one longitudinal and one transversal boson whereas the full sample is generated without differentiating between polarisations.

2.3.3 Comparing samples from WW and Parton Parton rest frames

As mentioned in section 1.3.2 the analytical functions are only expected to be accurate if the rest frame that the decay angle is calculated in fits the frame in which the helicity is defined. For the MadGraph samples this is the frame that the samples are generated in. To see whether the not ideal agreement between plots and analytical functions has to do with the samples being generated in the WW rest frame or maybe with the calculation of the decay angle in this frame, similar samples were generated in the Parton Parton rest frame. The decay angle in this frame was calculated as discussed in section 2.2.2. Figure 2.7 shows that there is indeed a shape difference between the two samples. The left plot shows the decay angle calculated in the WW rest frame for both the sample generated in that frame and the sample generated in the Parton Parton rest frame, the right plot shows the same for the angle calculated in the Parton Parton rest frame. It is noticeable that the shape difference between the two samples resembles the shape difference between the fitting function and the histogram in the left plot of figure 2.4: For the decay angle calculated in the WW rest frame for example, the WW rest frame sample is above the other sample near $\cos(\theta^*) = 1$ and $\cos(\theta^*) = -1$, but under the other sample for $\cos(\theta^*) = 0.2$. This could indicate that the bad quality of the fit might indeed have to do with the reference frames.

To find out whether the problem lies with the generation of samples or the calculation of the decay angle in the WW rest frame, the same fit was also performed for the sample generated in the Parton Parton rest frame, resulting in the left plot in figure A.9 and the fitting parameter $a = 0.3862 \pm 0.0019$ with $\chi^2_{red} = 7.581$. It is apparent that while being of slightly better quality, the fit shares the same problems as the one in the WW rest frame.

Just to rule out that the problem stems from confusing the samples generated in the two rest frames, the right plot in figure A.9 shows the same fit for the sample generated in the WW rest frame but with the decay angle calculated in the Parton Parton rest frame. As expected the agreement for this fit is even worse with a χ^2_{red} of $\chi^2_{red} = 23.607$.

As mentioned in section 1.3.2 the prediction also requires the absence of lepton cuts. Figure 2.9 shows the p_t of the leading lepton and it's pseudorapidity. These plots are exemplary for the lepton p_t and pseudorapidity plots for all the samples used in this thesis that are available in the appendix. The plots show no signs of cuts that were overlooked in the analysis or the generation of the events.

Unfortunately the issue could not be investigated any further due to the time limit of this thesis. Experts on the topic of event generation with the MadGraph software have been contacted, but the problem could not be resolved so far.

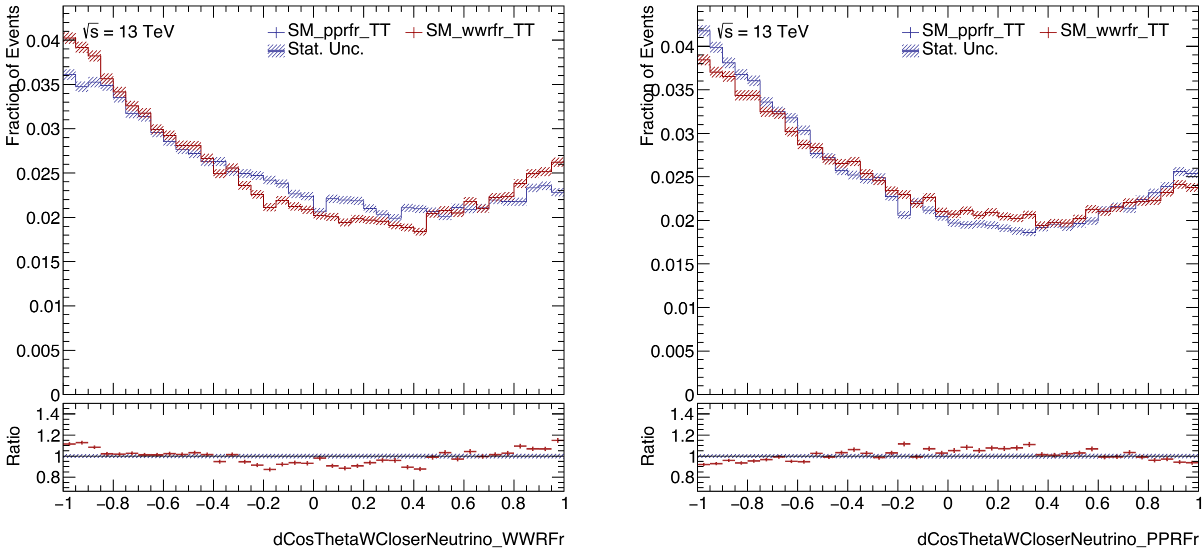

(a) cos of the decay angle θ_W^* as calculated in the WW rest frame.

(b) cos of the decay angle θ_W^* as calculated in the Parton Parton rest frame.

Figure 2.7: Comparing the differential cross section as a function of the cos of the decay angle θ_W^* for W^+ bosons in W^+W^+ vector boson scattering for two samples generated in the WW and the Parton Parton rest frame.

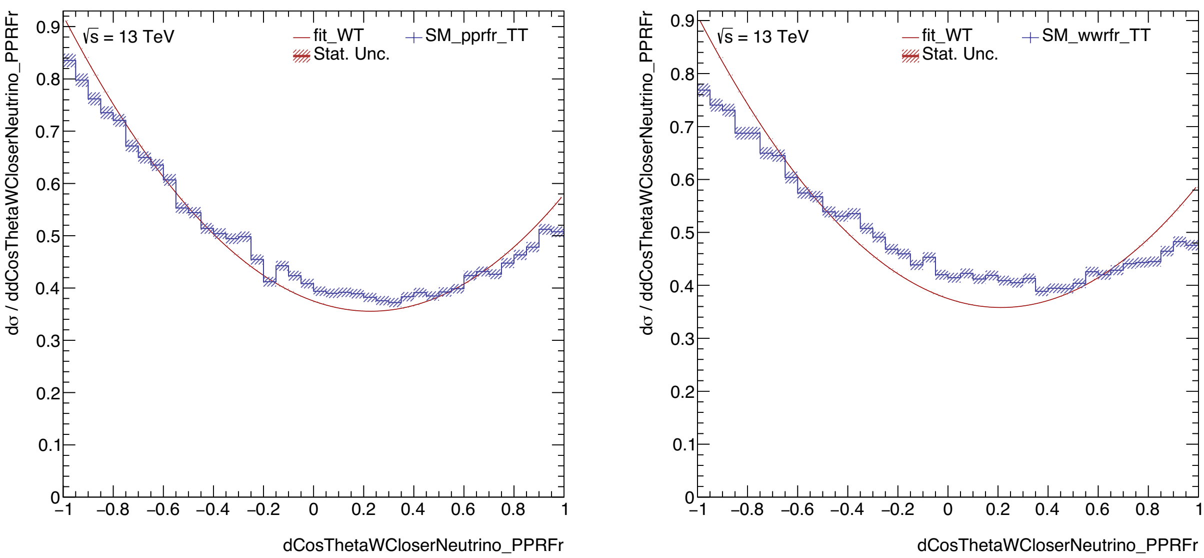

(a)

(b)

Figure 2.8: Differential cross section as a function of the cos of the decay angle θ_W^* for W^+ bosons in W^+W^+ vector boson scattering, including fitting functions. In plot (a) the angle was calculated in the Parton Parton rest frame, the same frame that the sample was generated in. Plot (b) shows the same sample but the variable is now the decay angle as calculated in the WW rest frame.

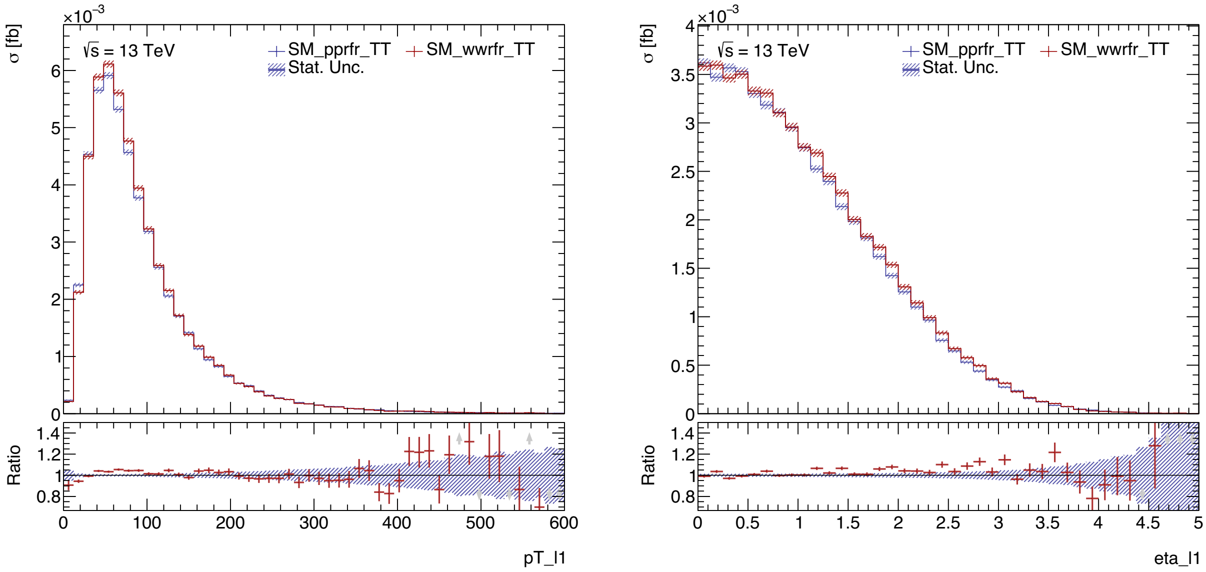

(a) **(b)**

Figure 2.9: Comparison of the leading lepton's p_t in GeV (a) and pseudo-rapidity (b) in W^+W^+ vector boson scattering for samples generated in the WW and the Parton Parton rest frame.

2.4 Results with EFT samples

As mentioned in section 1.4 the process of VBS is also a convenient starting point for the search for new physics using EFTs. The EFT samples generated for this thesis use a Lagrangian that compared to the Standard Model Lagrangian use an additional operator from the selection mentioned in section 1.4. The values that the respective parameters were set to are stated in 2.1.

As the EFT is fundamentally a way of describing unknown new physics beyond the energy scale that is accessible experimentally, the effect of the added operator is expected to be visible most clearly for indices with very high energies. This suggests that a plot of the invariant mass of the two W^+ bosons involved in the scattering would show an increased cross section for very high values of m_{WW} as compared to the Standard Model sample. The left plot in figure 2.10 shows that when comparing a sample that was produced with a non zero parameter for the T0 operator to a Standard Model one, this is indeed the case. A logarithmic scale has been chosen for this and many other plots in this section as it makes the difference in shape more visible.

As mentioned previously one of the inconvenient properties of WW same sign VBS specifically is the involvement of two neutrinos that are only recorded as missing transverse energy by the ATLAS detector. As the calculation of the invariant mass of the two bosons requires the reconstruction of the W masses, that variable is not the easiest choice when aiming to compare the simulation to real experimental data. Another, more accessible variable is the invariant mass of the two charged leptons, which is closely related to the invariant mass of the two bosons. The right plot in figure 2.10 shows that the invariant mass of the two charged leptons also exhibits an increased cross section at high invariant masses as compared to the Standard Model sample.

One of the expectations for the dimension eight operators that influence the VBS vertices is that certain ones only have an impact on vertices involving bosons with specific polarizations. Figure 2.11 compares the total cross section of the stacked polarization samples with T0 on the left side to the same histogram for the Standard Model sample on the right side. It clearly shows that the operator affects different polarizations differently, as the ratio between the three processes TT, LL and TL is shifted. Compared to the Standard Model sample, there is clearly an increased total cross section for the TT fraction. This is validated when comparing the polarization samples to the Standard Model sample separately. This is shown in figure 2.12 for the T0 operator. The three plots very clearly show that the T0 operator strongly influences the transversal indices, while the longitudinal and mixed processes remain essentially unchanged. Figure 2.13 shows the respective results for S1, which influences the longitudinal vertices, and figure 2.14 shows that the operator M0 influences mixed vertices. As mentioned in section 2.1, only M0 samples with opposite flavour leptons could be generated, whereas the Standard Model sample includes both same flavour and opposite flavour events. The Standard Model sample is still included in the plots of figure 2.14 as a reference, but the plots are normalized to make the shapes easier to compare.

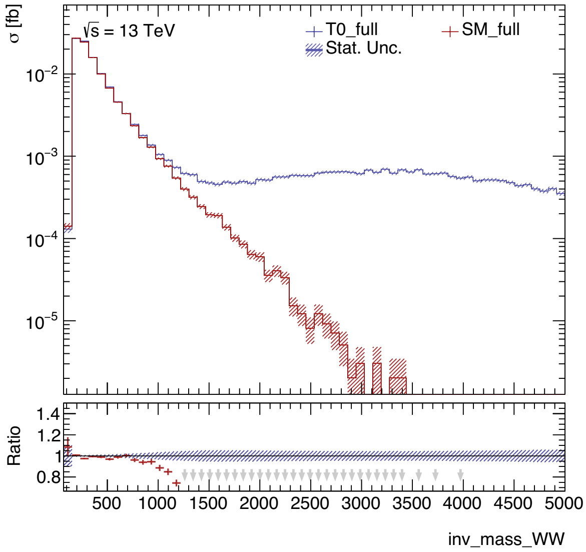

(a)

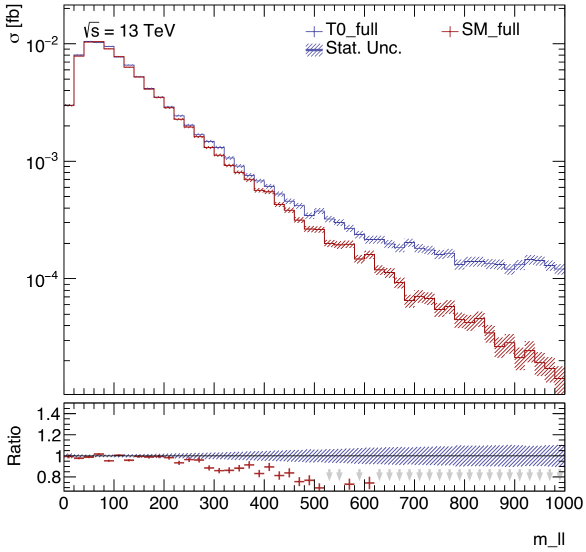

(b)

Figure 2.10: Effect of the introduction of the EFT operator T0 on the differential cross section as a function of the invariant mass of the W bosons (a) and the invariant mass of the two charged leptons m_{ll} (b), both in GeV, in vector boson scattering. The samples include the full process, in the generation of which the polarisations have not been separated.

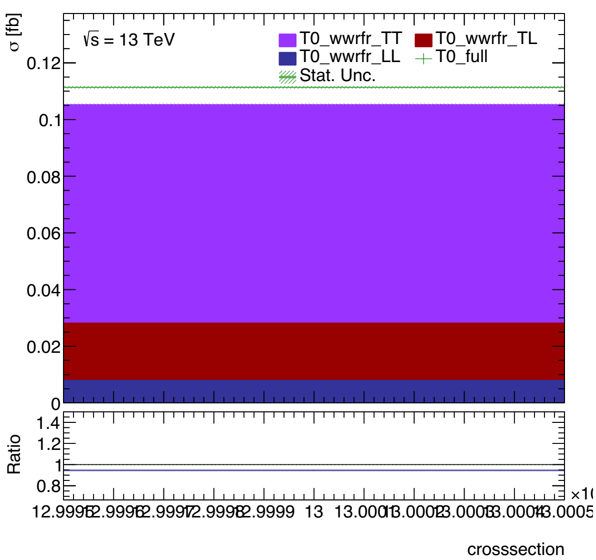

(a) Plot with T0 operator.

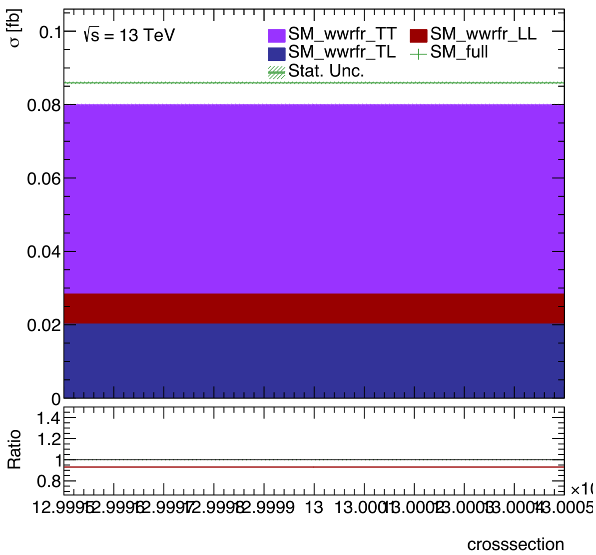

(b) Plot for Standard Model (all EFT parameters set to zero).

Figure 2.11: Effect of the introduction of the EFT operator T0 on the total cross section as a function of the invariant mass of the W bosons in W^+W^+ vector boson scattering. The plots compare the stack of the three polarisation samples TT, LL and TL (transversal, longitudinal and mixed) with the full process.

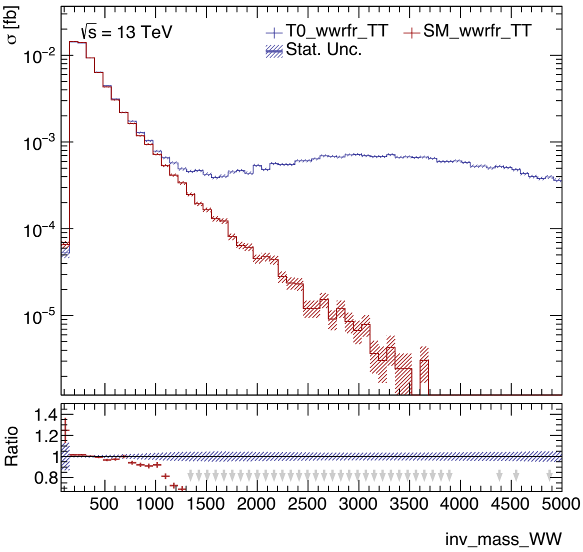

(a) Comparison between a SM and an EFT sample including vertices with two transversal W^+ bosons.

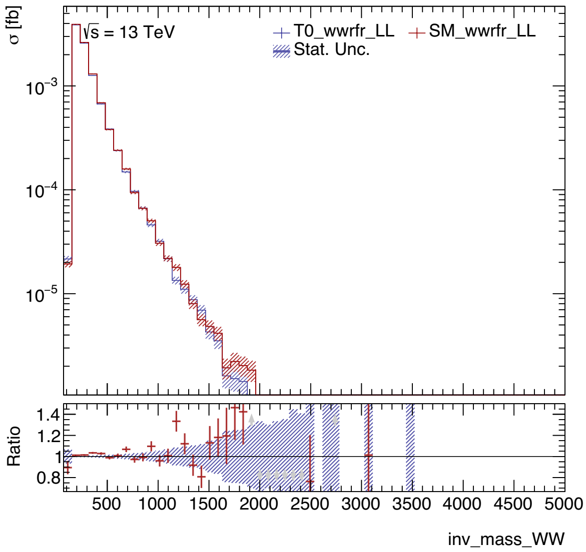

(b) Comparison between a SM and an EFT sample including vertices with two longitudinal W^+ bosons.

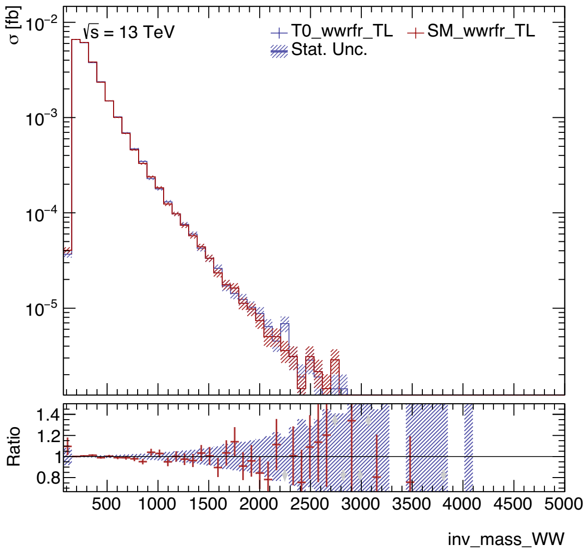

(c) Comparison between a SM and an EFT sample including vertices with one transversal and one longitudinal W^+ boson.

Figure 2.12: Effect of the introduction of the EFT operator T0 on the differential cross section as a function of the invariant mass of the W bosons in GeV in W^+W^+ vector boson scattering. The transversal, longitudinal and mixed vertices have been separated into three samples.

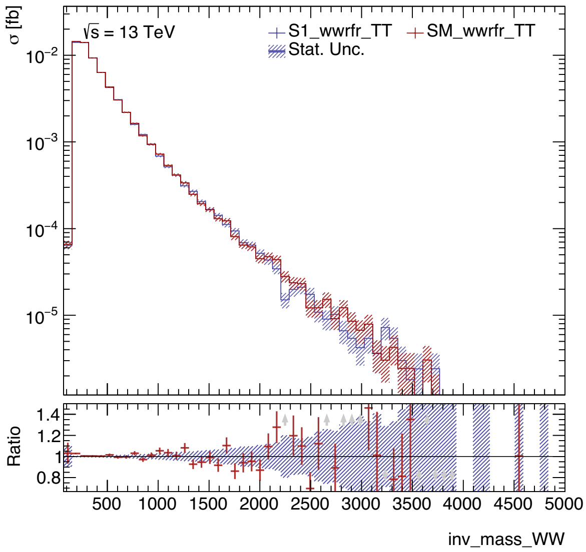

(a) Comparison between a SM and an EFT sample including vertices with two transversal W^+ bosons.

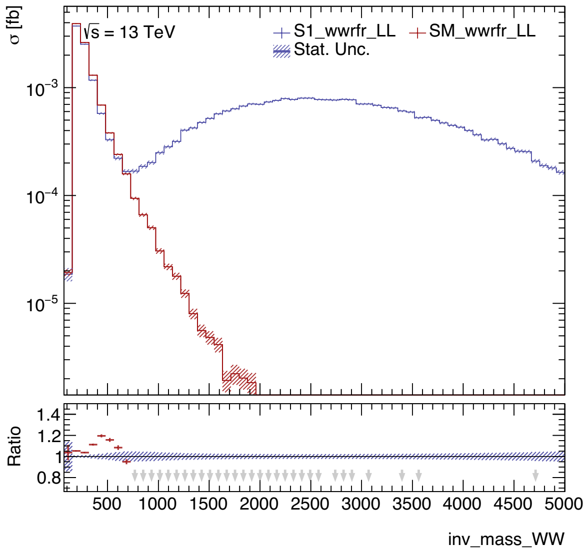

(b) Comparison between a SM and an EFT sample including vertices with two longitudinal W^+ bosons.

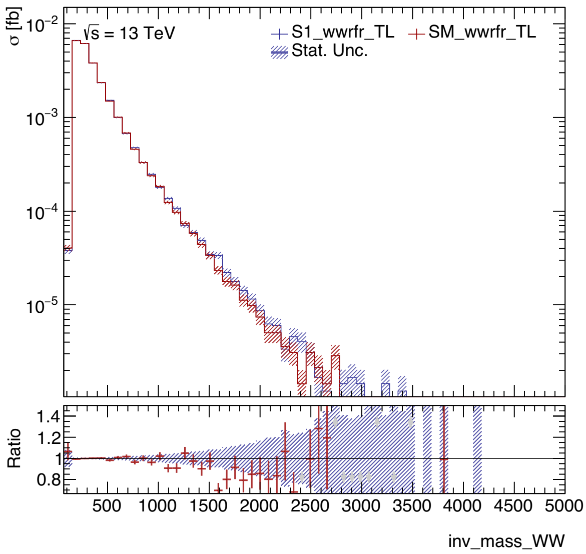

(c) Comparison between a SM and an EFT sample including vertices with one transversal and one longitudinal W^+ boson.

Figure 2.13: Effect of the introduction of the EFT operator S1 on the differential cross section as a function of the invariant mass of the W bosons in GeV in W^+W^+ vector boson scattering. The transversal, longitudinal and mixed vertices have been separated into three samples.

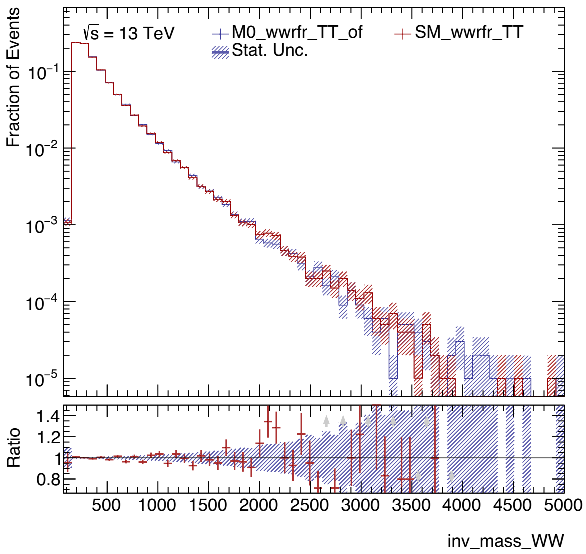

(a) Comparison between a SM and an EFT sample including vertices with two transversal W^+ bosons.

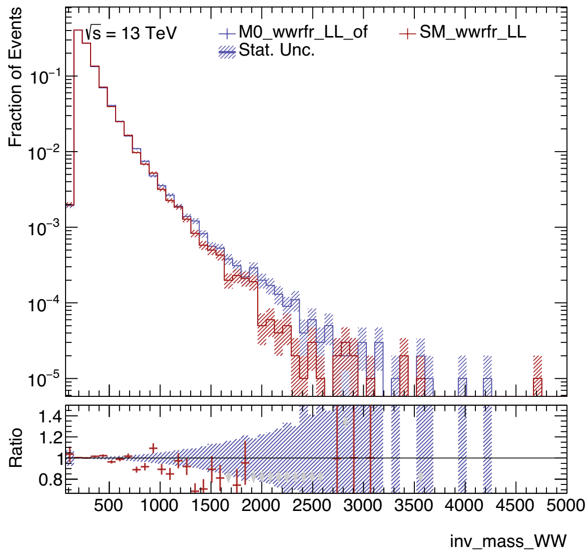

(b) Comparison between a SM and an EFT sample including vertices with two longitudinal W^+ bosons.

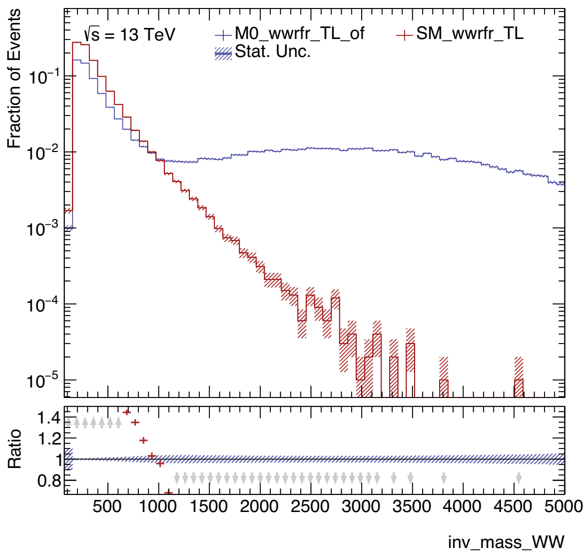

(c) Comparison between a SM and an EFT sample including vertices with one transversal and one longitudinal W^+ boson.

Figure 2.14: Effect of the introduction of the EFT operator M0 on the differential cross section as a function of the invariant mass of the W bosons in GeV in W^+W^+ vector boson scattering. The transversal, longitudinal and mixed vertices have been separated into three samples. The SM sample includes events with the W^+ bosons decaying into a muon and an electron as well as ones with the bosons decaying into two muons or two electrons. The M0 sample includes only opposite flavour events, which means there is a difference in the total cross section between the two. In order to make their shapes comparable, the plots are normalized.

3 Summary and Outlook

The process of vector boson scattering is an area of active and ongoing research, that provides insight into both the details of the Standard Model and the possibility of new physics beyond it. The results for Standard Model samples confirm that the relationship between the rest frame in which the events are generated and the exact definition of the boson decay angle is important to the shape of the differential cross section. Unfortunately the expected behaviour could not be exactly replicated. As of the end of this study, the reason for this is still unknown. The technical difficulties in the generation of the samples as well as similar observations in the related process of WZ vector boson scattering do imply that the fault is likely to do with the generated simulation data or the specific Rivet analysis used. Experts on the issue have been contacted, and the problem will be further investigated.

This thesis focused on the comparison of simulation data to the expected behaviour for the W decay angle θ^*_W specifically. As discussed earlier this is not a variable that is easily accessible in experiment. In order to use the vector boson scattering process to it's full potential however, the polarisation of the bosons needs to be studied in real experimental data. This requires further research into possible variables that are sensitive to the polarisations at the scattering vertex, but are also more accessible by the experiment.

The results on EFT parameters presented in this thesis can only be described as a very small glimpse into the possible effects of these new operators in the Lagrangian of the model. It is visible in the simulation data produced using the software model mentioned in 2.1, that the chosen dimension eight operators do indeed only influence either transversal, longitudinal or mixed vertices within the process. Limiting the EFT to one dimension eight operator at a time however means sacrificing the great advantage of model independence as an exchange for simplicity. Additionally, recent research [5] suggests that the effect of dimension eight operators, the impact of dimension six operators on vector boson scattering is not negligible. This means that a much more detailed, in-depth study than is possible here would be required to accurately model the impact of an EFT on the process.

A Plots showing no lepton cuts

A discussed in section 2.3.3, one of the requirements for the agreement between the analytical expectation and the simulation data of the differential cross section as a function of the boson decay angle is that no lepton cuts are applied to the decay products of the W^+ bosons. To check whether this is the case and no cuts in the generation process or the analysis were overlooked, the following figures show the transversal momentum p_t and pseudorapidity η of the leptons from the relevant samples. The plots show that no cuts were applied to the leptons, as no sudden cut-offs are visible.

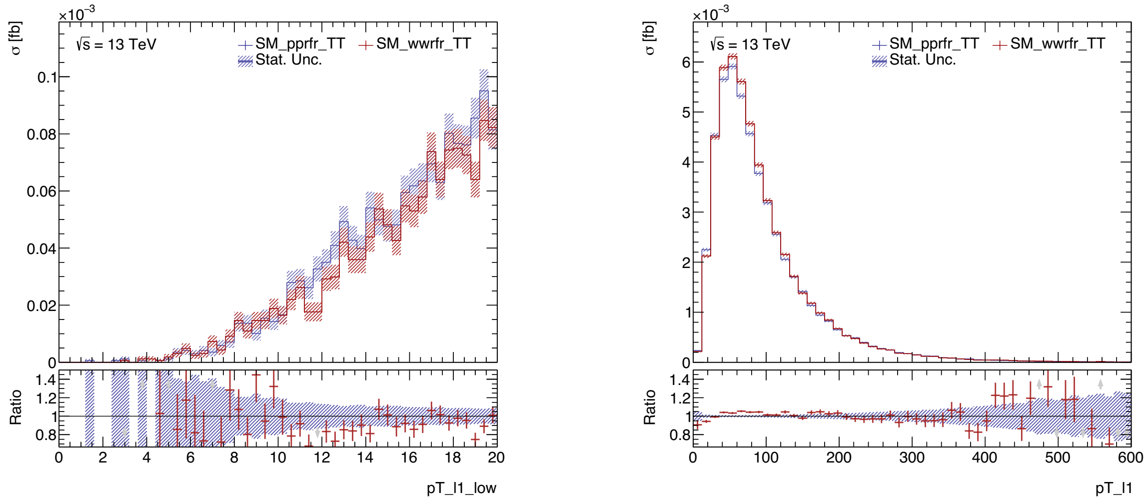

(a) Close-up of the low p_t region. **(b)** Overview of the entire p_t distribution.

Figure A.1: Lepton p_t in GeV for the leading lepton in W^+W^+ vector boson scattering, comparing a sample generated in the WW and one in the Parton Parton rest frame. Both include only vertices with two transversal W^+ bosons.

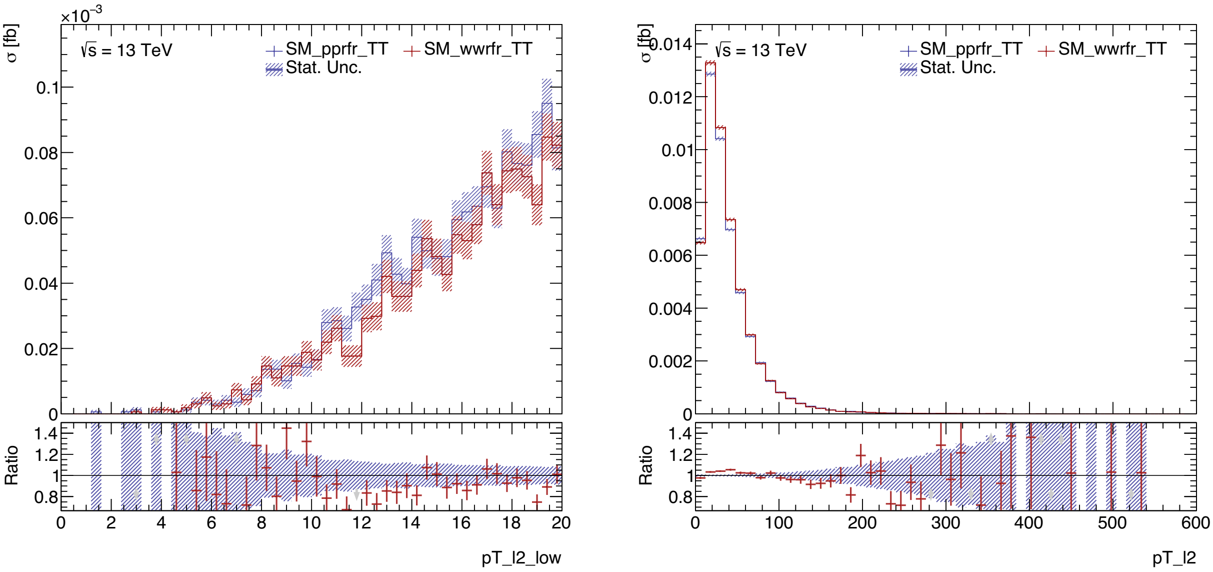

(a) Close-up of the low p_t region. **(b)** Overview of the entire p_t distribution.

Figure A.2: Lepton p_t in GeV for the subleading lepton in W^+W^+ vector boson scattering, comparing a sample generated in the WW and one in the Parton Parton rest frame. Both include only vertices with two transversal W^+ bosons.

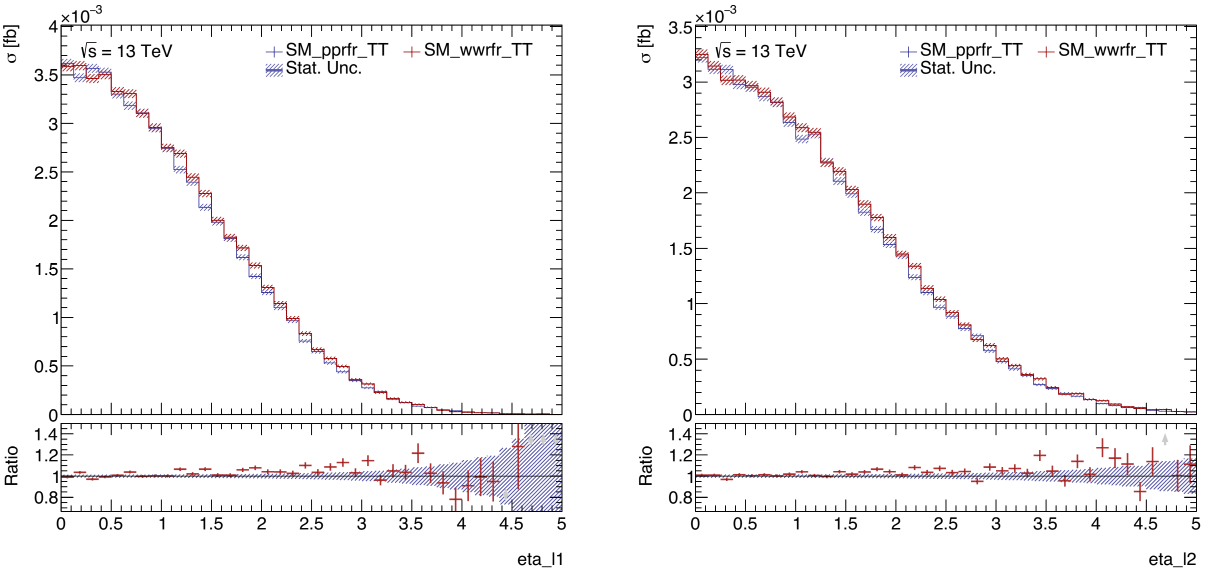

(a) **(b)**

Figure A.3: Pseudorapidity for the leading (a) and subleading (b) leptons in W^+W^+ vector boson scattering, comparing a sample generated in the WW and one in the Parton Parton rest frame. Both include only vertices with two transversal W^+ bosons.

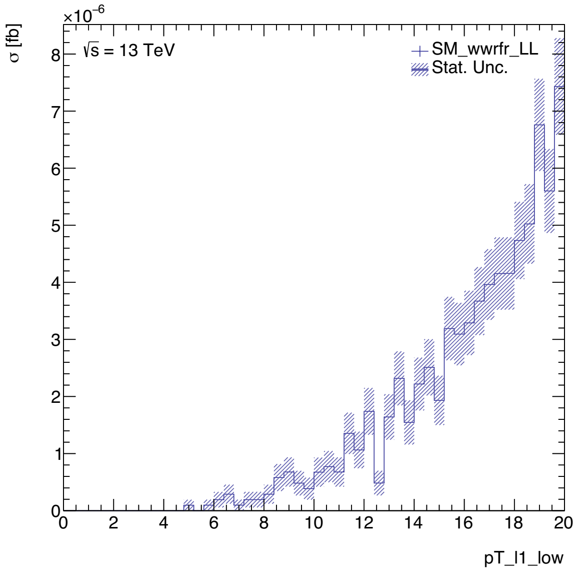

(a) Close-up of the low p_t region.

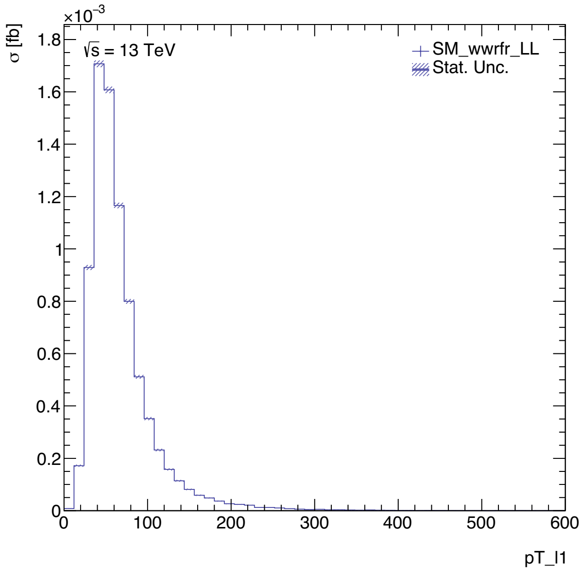

(b) Overview of the entire p_t distribution.

Figure A.4: Lepton p_t in GeV for the leading lepton in W^+W^+ vector boson scattering. The sample was generated in the WW rest frame and includes only vertices with two longitudinal W^+ bosons.

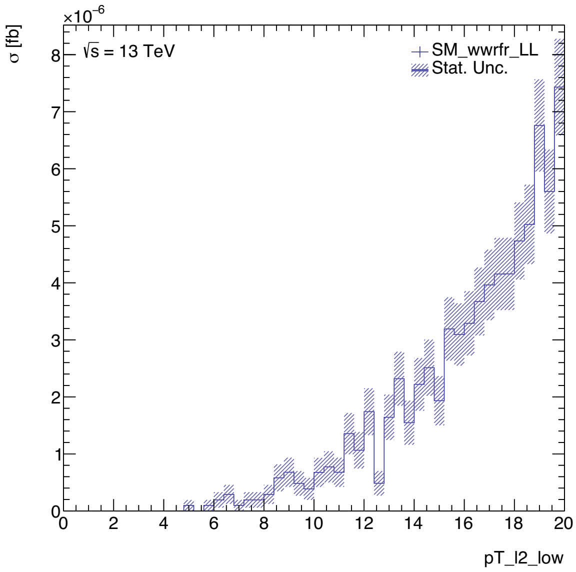

(a) Close-up of the low p_t region.

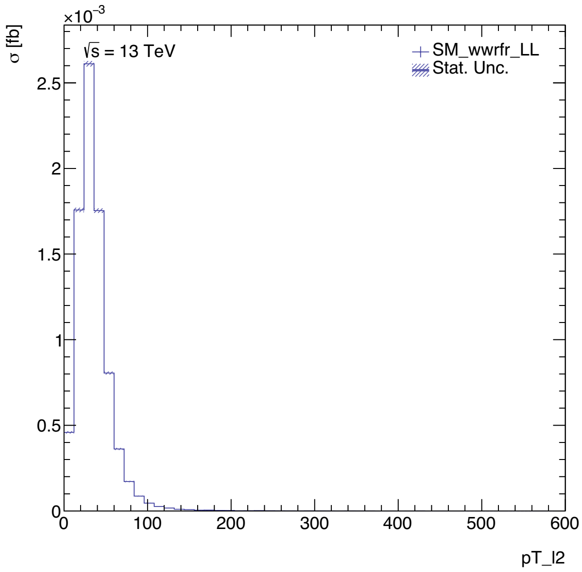

(b) Overview of the entire p_t distribution.

Figure A.5: Lepton p_t in GeV for the subleading lepton in W^+W^+ vector boson scattering. The sample was generated in the WW rest frame and includes only vertices with two longitudinal W^+ bosons.

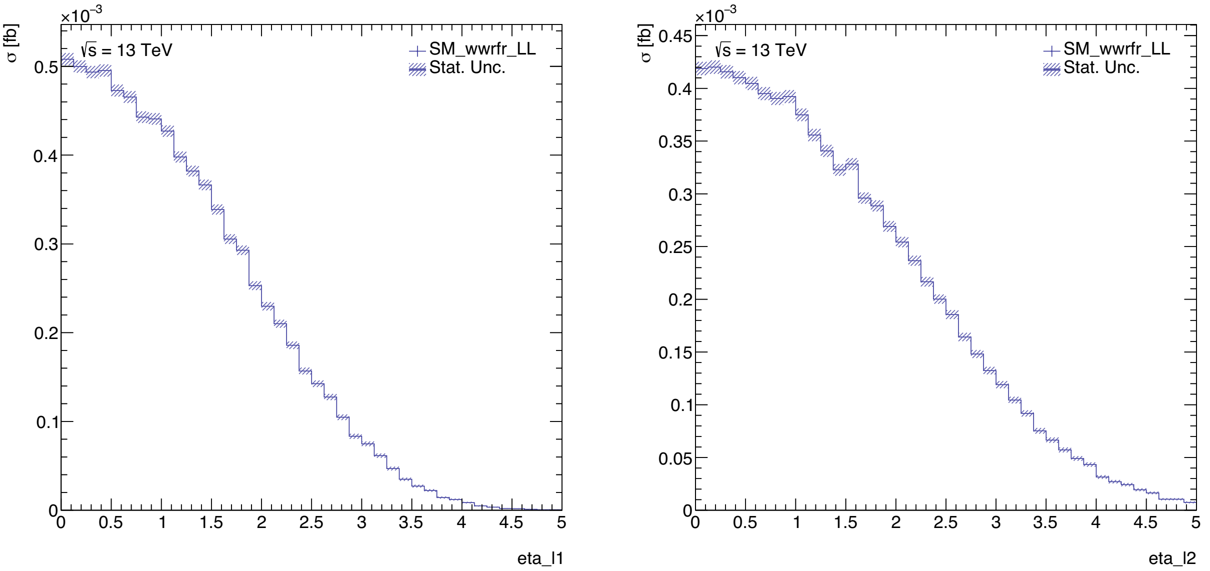

(a) **(b)**

Figure A.6: Lepton pseudorapidity for the leading (a) and subleading (b) leptons in W^+W^+ vector boson scattering. The sample was generated in the WW rest frame and only includes vertices with two longitudinal W^+ bosons.

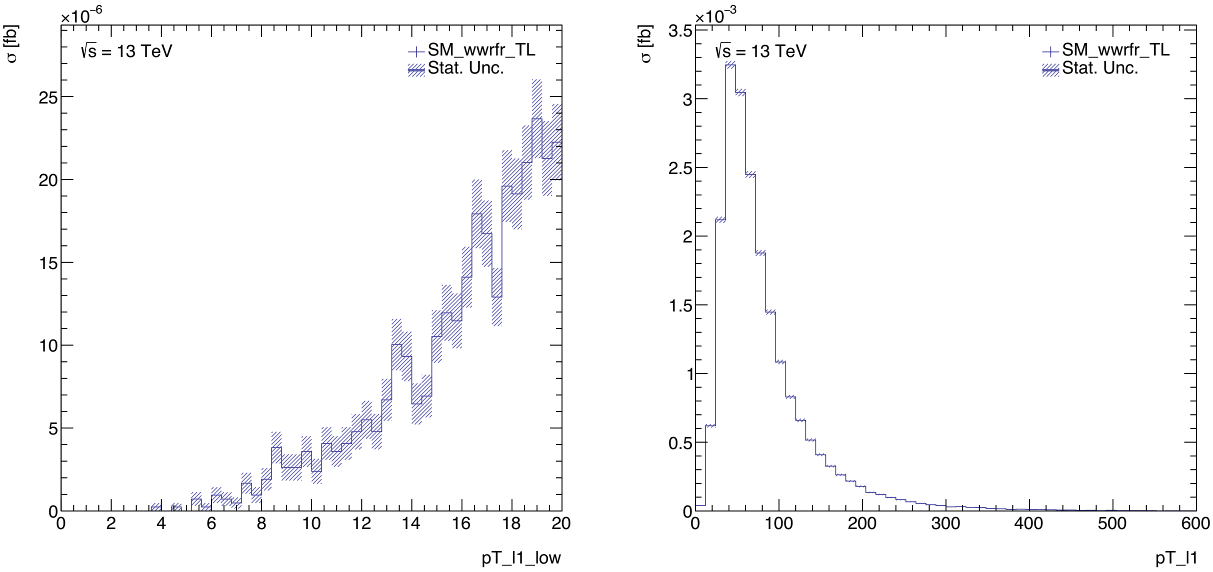

(a) Close-up of the low p_t region. **(b)** Overview of the entire p_t distribution.

Figure A.7: Lepton p_t in GeV for the leading lepton in W^+W^+ vector boson scattering. The sample was generated in the WW rest frame and includes only vertices with one transversal and one longitudinal W^+ boson.

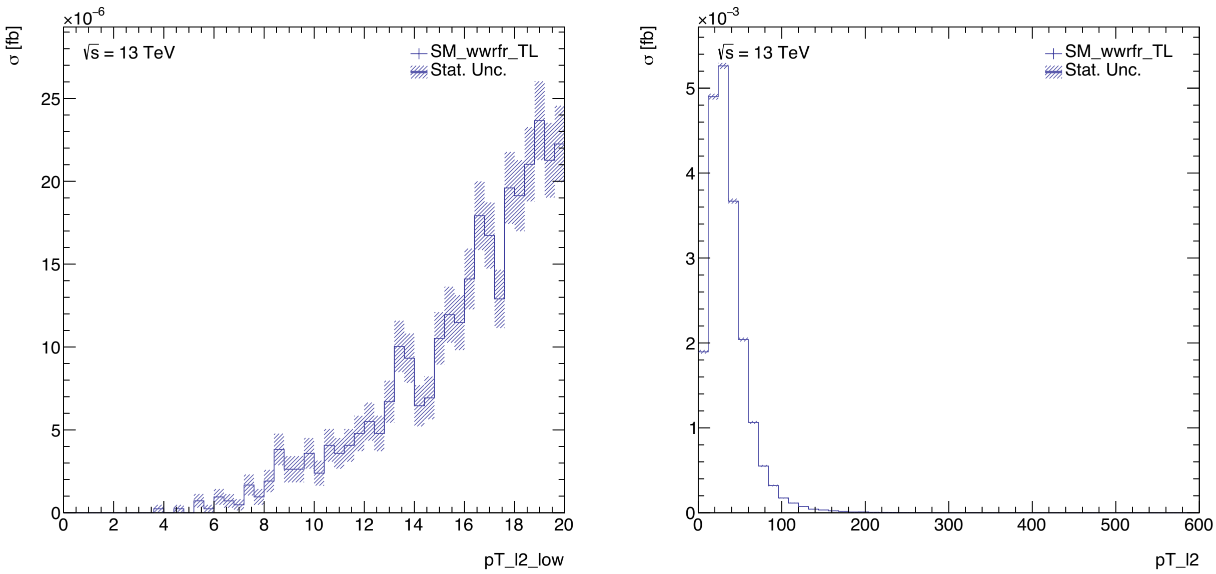

(a) Close-up of the low p_t region.

(b) Overview of the entire p_t distribution.

Figure A.8: Lepton p_t in GeV for the subleading lepton in W^+W^+ vector boson scattering. The sample was generated in the WW rest frame and includes only vertices with one transversal and one longitudinal W^+ boson.

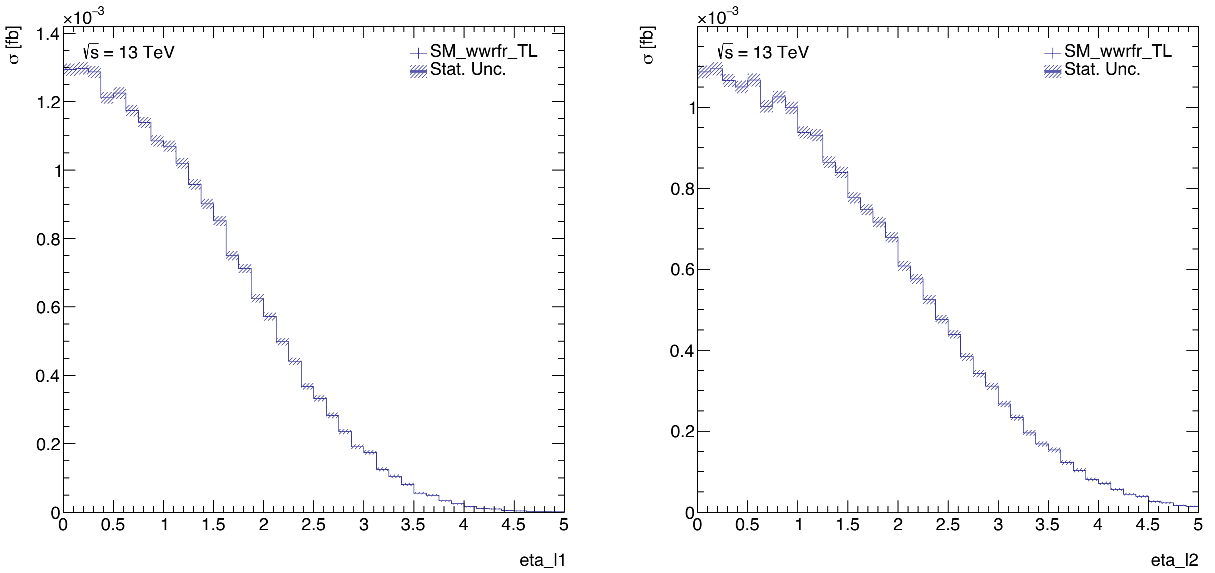

(a)

(b)

Figure A.9: Lepton pseudorapidity for the leading (a) and subleading (b) leptons in W^+W^+ vector boson scattering. The sample was generated in the WW rest frame and only includes vertices with two longitudinal W^+ bosons.

B Bibliography

[1] L. Evans and P. Bryant, "LHC Machine", *Journal of Instrumentation*, vol. 3, no. 08, S08001–S08001, Aug. 2008. DOI: 10.1088/1748-0221/3/08/s08001. [Online]. Available: https://doi.org/10.1088%2F1748-0221%2F3%2F08%2Fs08001.

[2] ATLAS Collaboration, "Observation of a new particle in the search for the Standard Model Higgs boson with the ATLAS detector at the LHC", *Physics Letters B*, vol. 716, pp. 1–29, Sep. 2012. DOI: 10.1016/j.physletb.2012.08.020.

[3] C. Bittrich, "Study of Polarization Fractions in the Scattering of Massive Gauge Bosons W±Z → W±Z with the ATLAS Detector at the Large Hadron Collider", Master's Thesis, Technische Universität Dresden, 2015.

[4] A. Pich, "Effective Field Theories", 1998. [Online]. Available: https://arxiv.org/abs/hep-ph/9806303.

[5] A. Dedes, P. Kozów, and M. Szleper, "SM EFT effects in Vector-Boson Scattering at the LHC", 2020.

[6] D. Griffiths, *Introduction to Elementary Particles.* Wiley-VCH Verlag, 2008.

[7] ATLAS Collaboration, "Evidence for Electroweak Production of W±W±jj in pp Collisions at s$\sqrt{s}$=8 TeV with the ATLAS Detector", *Physical review letters*, vol. 113, p. 141 803, Oct. 2014. [Online]. Available: https://arxiv.org/abs/1405.6241.

[8] R. G. Ambrosio, "Studies of Gauge Couplings at LHC: the Effective Field Theory Approach", PhD, Università degli Studi di Torino, 2017.

[9] J.-E. Nitschke, "Studies on polarization in the scattering of two vector bosons with the ATLAS experiment at the LHC", Master's Thesis, Technische Universität Dresden, 2019.

[10] W. Stirling and E. Vryonidou, "Electroweak gauge boson polarisation at the LHC", *Journal of High Energy Physics*, vol. 124 (2012), [Online]. Available: https://doi.org/10.1007/JHEP07(2012)124.

[11] U. Schnoor, "Electroweak Production of Two Like-Charge W Bosons and Two Jets at the Current and Future ATLAS Detector", PhD thesis, Technische Universität Dresden, 2014. [Online]. Available: http://cds.cern.ch/record/2000941/files/CERN-THESIS-2014-281-rev.pdf.

[12] M. Sekulla, "Anomalous Couplings, Resonances and Unitarity in Vector Boson Scattering", PhD Thesis, Universität Siegen, 2015. [Online]. Available: https://nbn-resolving.org/urn:nbn:de:hbz:467-9793.

[13] S. Todt, "Quartic Couplings in $W^{\pm}W^{\pm}$ Scattering with the ATLAS Detector at the LHC", Unpublished PhD thesis, Technische Universität Dresden, 2020.

[14] The ATLAS Collaboration, "The ATLAS Experiment at the CERN Large Hadron Collider", *Journal of Instrumentation*, vol. 3, no. 08, S08003–S08003, Aug. 2008. DOI: 10.1088/1748-0221/3/08/s08003. [Online]. Available: https://doi.org/10.1088%2F1748-0221%2F3%2F08%2Fs08003.

[15] (2020). "Launchpad for MadGraph5_aMC@NLO", [Online]. Available: https://launchpad.net/mg5amcnlo.

[16] O. Eboli and M. Gonzalez-Garcia. (2020). "Anomalous quartic electroweak gauge-boson interactions", [Online]. Available: https://feynrules.irmp.ucl.ac.be/wiki/AnomalousGaugeCoupling.

[17] O. J. P. Éboli and M. C. Gonzalez–Garcia, "Classifying the bosonic quartic couplings", *Physical Review D*, vol. 93, no. 9, May 2016, ISSN: 2470-0029. DOI: 10.1103/physrevd.93.093013. [Online]. Available: http://dx.doi.org/10.1103/PhysRevD.93.093013.

[18] (2020). "Website of the VBSCan Action", [Online]. Available: https://vbscanaction.web.cern.ch.

Erklärung

Hiermit erkläre ich, dass ich diese Arbeit im Rahmen der Betreuung am Institut für Kern- und Teilchenphysik ohne unzulässige Hilfe Dritter verfasst und alle Quellen als solche gekennzeichnet habe.

M. Bühring

Maren Bühring
Dresden, 01. Dezember 2020